












Doppler and sympathetic cooling for the investigation of short-lived radioactive ions

S. Sels ^{1,2,*} F. M. Maier^{1,3} M. Au ^{1,4} P. Fischer ³ C. Kanitz¹ V. Lagaki ^{1,3} S. Lechner ^{1,5} E. Leistenschneider ¹
D. Leimbach ^{1,6,7} E. M. Lykiardopoulou^{8,9} A. A. Kwiatkowski⁸ T. Manovitz ¹⁰ Y. N. Vila Gracia¹ G. Neyens ^{1,2}
P. Plattner ^{1,11} S. Rothe¹ L. Schweikhard³ M. Vilen¹ R. N. Wolf ¹² and S. Malbrunot-Ettenauer¹

¹CERN, CH-1211 Geneve 23, Switzerland

²Instituut voor kern- en stralingsfysica, KU Leuven, Celestijnenlaan 200D, Leuven, Belgium

³Institut für Physik, Universität Greifswald, 17487 Greifswald, Germany

⁴Johannes Gutenberg-Universität Mainz, Department Chemie, Standort TRIGA, Fritz-Strassmann-Weg 2, 55128 Mainz, Germany

⁵Technische Universität Wien, Karlsplatz 13, 1040 Wien, Austria

⁶Department of Physics, University of Gothenburg, SE-412 96 Gothenburg, Sweden

⁷Institut für Physik, Johannes Gutenberg-Universität, 55099 Mainz, Germany

⁸TRIUMF, 4004 Wesbrook Mall, Vancouver, British Columbia, Canada V6T 2A3

⁹Department of Physics and Astronomy, University of British Columbia, Vancouver, British Columbia, Canada V6T 1Z1

¹⁰Department of Physics of Complex Systems, Weizmann Institute of Science, Rehovot 76100, Israel

¹¹Universität Innsbruck, Innrain 52, 6020 Innsbruck, Austria

¹²ARC Centre of Excellence for Engineered Quantum Systems, The University of Sydney, New South Wales 2006, Australia



(Received 9 February 2022; accepted 15 June 2022; published 23 September 2022)

At radioactive ion beam (RIB) facilities, ions of short-lived radionuclides are cooled and bunched in buffer-gas-filled Paul traps to improve the ion-beam quality for subsequent experiments. To deliver even colder ions, beneficial to RIB experiments' sensitivity or accuracy, we employ Doppler and sympathetic cooling in a Paul trap cooler-buncher. The improved emittance of Mg^+ , K^+ , and O^+ ion beams is demonstrated by a reduced time-of-flight spread of the extracted ion bunches with respect to room-temperature buffer-gas cooling. Cooling externally-produced hot ions with energies of at least 7 eV down to a few Kelvin is achieved in a timescale of $O(100 \text{ ms})$ by combining a low-pressure helium background gas with laser cooling. This is sufficiently short to cool short-lived radioactive ions. As an example of this technique's use for RIB research, the mass-resolving power in a multireflection time-of-flight mass spectrometer is shown to increase by up to a factor of 4.6 with respect to buffer-gas cooling. Simulations show good agreement with the experimental results and guide further improvements and applications. These results open a path to a significant emittance improvement and, thus, unprecedented ion-beam qualities at RIB facilities, achievable with standard equipment readily available. The same method provides opportunities for future high-precision experiments with radioactive cold trapped ions.

DOI: [10.1103/PhysRevResearch.4.033229](https://doi.org/10.1103/PhysRevResearch.4.033229)

I. INTRODUCTION

Radioactive ion beam (RIB) facilities around the world specialize in producing beams of short-lived radioactive nuclides for a broad range of scientific experiments [1–9]. Studies of these exotic radionuclides extend our knowledge of the nuclear forces which bind protons and neutrons together to form atomic nuclei, guide nuclear astrophysics in its understanding of the formation of the chemical elements, and enable precision experiments on nuclear probes to search for new physics beyond the standard model of particle physics [10–12]. Moreover, modern RIB facilities play a central role in nuclear applications for solid state, bio-, and medical

physics, in particular, in the quest for innovative medical isotopes [13–16].

To meet the ion-beam requirements of RIB experiments, ions are often cooled and bunched to improve the beam quality before being transported to dedicated experimental instruments. Typically, this cooling is performed by buffer-gas-filled linear Radio Frequency (RF) ion traps, also called Paul traps [17–25]. In the context of RIB facilities, these ion traps are commonly referred to as cooler bunchers. They are able to capture, accumulate, bunch, cool, and eject virtually all species of ions, making them versatile and often indispensable tools. The cooling limit achievable in such a linear Paul trap is on the order of the buffer-gas temperature [26–28]. In most operational cooler-bunchers at RIB facilities, this corresponds to room temperature of about 300 K, and a few instruments can operate at liquid nitrogen temperature [21,29].

However, in other fields of research, experiments take advantage of much colder ensembles. For instance, laser cooling of trapped neutral and ionized atoms and molecules has revolutionized the field of experimental quantum physics. Since its inception in the 1970s [30–33], it has been a

*Simon.Sels@cern.ch

Published by the American Physical Society under the terms of the [Creative Commons Attribution 4.0 International](https://creativecommons.org/licenses/by/4.0/) license. Further distribution of this work must maintain attribution to the author(s) and the published article's title, journal citation, and DOI.

cornerstone in several Nobel-prize-winning experiments [33–35] as it allows for a precise preparation and quantum coherent control of cold trapped atoms and molecules. In the meantime, various laser-cooling techniques have been developed [36] and laser cooling has become a standard tool for high-precision research and applications such as atomic clocks [37], quantum information science [38], the search for physics beyond the standard model [39], and the study of anti-matter [40,41]. In contrast to buffer-gas cooling, temperatures achievable with Doppler laser cooling [36] are several orders of magnitude lower and only restricted by the Doppler cooling limit, $T = \hbar\Gamma/2k_B$ [42]. Here, \hbar is the reduced Planck's constant, Γ is the atomic transition linewidth, and k_B is Boltzmann's constant. For instance, in singly charged magnesium ions, the cooling limit becomes $T \approx 1$ mK when utilizing the D1 and D2 cooling transitions [43].

The beam quality of an ion bunch extracted from a Paul trap, expressed quantitatively as the ion beam emittance, scales with the temperature of the ion ensemble [44]. The relation between the temperature T of cooled, trapped ions and the longitudinal emittance of a subsequently extracted ion bunch can be quantified at the time-focus point in terms of the latter's energy spread ΔE and temporal width Δt , following [21]

$$(\Delta E \Delta t)_{95\%} \approx 2\pi \ln(20) k_B T \sqrt{\frac{m}{2qC_2}}. \quad (1)$$

Here, m and q represent the mass and charge of the ions, respectively, while the trapping parameter C_2 is related to the axial trap depth (for details, see Ref. [21]).

Next-generation experiments at RIB facilities will have increased demands on the quality of the RIBs. In this context, laser cooling could provide the necessary reduction of ion temperature for the formation of RIBs with hitherto unmatched qualities. By way of sympathetic cooling of cotrapped (radioactive) ions, this temperature reduction will not be limited to the few laser-coolable ions, but will lead to a universal availability of cold RIBs of any atomic or molecular species.

In this paper, we report on direct laser cooling of magnesium ions and sympathetic cooling of cotrapped atomic and molecular ions in a Paul-trap cooler-buncher with the goal of improving ion-beam emittance within a timescale that is compatible with experiments involving short-lived radioactive ions. To this end, we systematically study the properties of extracted ion bunches following laser and sympathetic cooling in the ion trap. Our results show a significantly reduced temporal ion-bunch width, indicating an improved longitudinal beam emittance with respect to room-temperature buffer-gas cooled ion bunches. The experimental results are in good agreement with accompanying three-dimensional (3D) cooling simulations of the experimental setup and procedures. In addition, these simulations are benchmarked against a one-dimensional (1D) numerical cooling model. Both tools, 3D simulation and the 1D model, are employed to extend the cooling dynamics beyond the experimentally accessible ion-bunch properties. Thereby, we are able to envision and study applications of this cooling method for various RIB experiments.

Laser-cooled ion bunches at RIB facilities will allow for an increased sensitivity in collinear laser spectroscopy experiments on exotic atoms or molecules [10,45–47]. Likewise,

this cooling scheme will increase the resolving power of mass measurements of radionuclides. First, we experimentally demonstrate the latter by inserting a laser-cooled ion bunch into a multireflection time-of-flight mass spectrometer (MR-ToF MS) [48–50], resulting in an improved mass-resolving power. Second, we simulate how this cooling technique can be used for the phase-imaging ion-cyclotron resonance (PI-ICR) method in Penning-trap-based mass measurements [51,52]. Here, the simulation results promise an improvement in precision of up to two orders of magnitude. Finally, we show, as an experimental validity check, that this cooling technique can also be used for measuring isotope shifts between different laser-coolable isotopes by observing the time-of-flight (ToF) width of the extracted ion bunches as a function of cooling-laser frequency.

Laser cooling at RIB facilities has been utilized for dedicated trapped-ion or atom experiments [2,53–58], but never, to our knowledge, for the delivery of high-quality (short-lived) ion beams. Like-minded applications of laser cooling have recently been pursued for improving the mass-resolving power $R = m/\Delta m$ for ToF mass separation of stable nuclides [59–62]. Our paper distinguishes itself in two aspects: First, we report on the improvement of R by another two orders of magnitude enabled by our unique combination of laser cooling and MR-ToF mass spectrometry. Second, and more importantly, we focus on laser-cooling applications of externally produced hot ions, as is the case for cooler bunches at RIB facilities. More generally, our paper discusses the potential use of laser and sympathetic cooling for various RIB experiments and demonstrates the feasibility of cooling hot, energetic ions to few-Kelvin temperatures within time constraints imposed by experiments with short-lived radionuclides. We thus propose this technique for future cooling of RIBs. As demonstrated in the present paper, by utilizing an unmodified cooler buncher, many laser-cooling applications can be readily implemented in existing linear Paul traps at RIB facilities despite their original design being focused on buffer-gas cooling. In fact, buffer-gas cooling at low gas pressures followed by laser cooling represents an attractive combination to reduce the temperature of hot injected ions (demonstrated here for $E > 7$ eV at the entrance of the Paul trap) to (sub-)Kelvin level within a timescale compatible with half-lives of radionuclides with $T_{1/2} < 1$ s. We also note the significance of this step for future cold trapped-ion experiments at RIB facilities. Cooling techniques, analogous to the ones demonstrated in this paper, are critical prerequisites for laser-spectroscopy experiments on cold trapped ions with short-lived radioactive isotopes which aim to improve on the current precision frontier in nuclear structure or beyond-standard-model physics, as, for example, in fifth-force searches from precision isotope-shift measurements [63,64].

II. EXPERIMENTAL SETUP AND METHOD

The main components of the experimental setup, sketched in Fig. 1, are two ion sources that provide low-energy beams of either magnesium (Mg^+) or potassium (K^+) ions and are connected via a quadrupole bender to a linear segmented Paul-trap cooler buncher, an MR-ToF device, and the laser

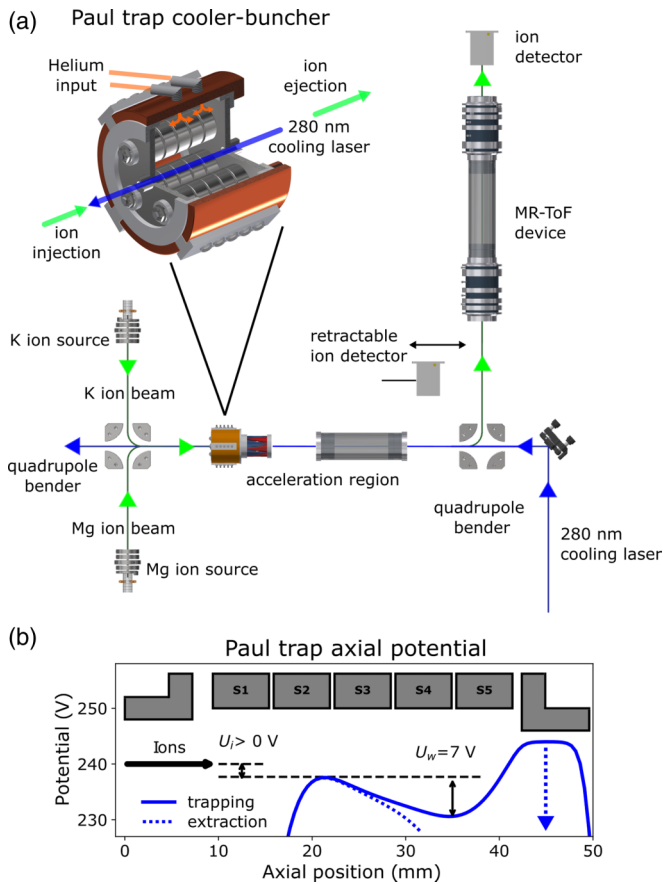


FIG. 1. (a) Layout of the experimental setup showing the main components with an enlarged, detailed view of the Paul trap cooler buncher. There, Mg^+ ions are Doppler cooled by 280-nm laser light for direct or sympathetic laser cooling of other ions species. See text for details. (b) dc potential along the Paul-trap axis during trapping (solid blue) and extraction (dashed blue). The position of the individual dc trap electrodes is indicated in gray. The axial well depth U_w and ions' excess energy U_i are shown as vertical arrows.

system. This apparatus is part of the MIRACLS project at CERN-ISOLDE, detailed in previous publications [65–69].

Singly charged ions of stable magnesium isotopes, $^{24,25,26}Mg^+$, with relative natural abundances of approximately 80, 10, and 10%, respectively, are produced by electron-impact ionization of magnesium vapor from a resistively heated crucible [70], similar to Ref. [71]. The positively charged Mg^+ ions are extracted from the ion source by a 240-V potential difference. When another species is co-trapped with the magnesium ions, they can either be ionized simultaneously in the same ion source or can be delivered by a separate surface ion source of the standard ISOLDE design [72–74]. The former is used in the case of dioxygen ions O_2^+ , where the ion source is operated under different conditions and the latter is utilized for the production of singly charged potassium ions, K^+ . After extraction from the ion source(s), the ions pass into a 90° electrostatic quadrupole bender which is controlled by high-voltage (HV) switches to selectively deflect ions from one of the two ion sources toward the Paul trap.

The Paul trap cooler buncher consists of four rods that provide the RF fields for radial ion confinement. They are each

split into five longitudinal segments of equal length to which additional dc voltages are applied to create an axial potential well. The characteristic Paul-trap dimension r_0 of the minimum distance of the rod surfaces to the trap axis is 6.2 mm. The trap is operated in ac-only mode at an RF frequency of 2 MHz and voltage amplitude of 140 V. Surrounding the Paul trap electrodes is a grounded metallic housing for spatial confinement of the helium buffer gas as well as two end-cap electrodes with a 4 mm (2 mm) diameter aperture for injection (extraction) of ions.

An electrostatic steerer upstream of the Paul trap, controlled by a HV switch, acts as a beamgate; i.e., ions pass into the cooler buncher during a well-defined ion-loading time. This loading time typically ranges from $10 \mu s$ to 500 ms. Subsequently, the ion beam is deflected away from the ion trap's entrance. The period after ion injection, during which no additional ions are entering the trap, is referred to as cooling time.

In full analogy to cooler bunchers at RIB facilities, the Paul-trap electrodes are floated to a potential just below the ions' initial acceleration potential. This reduces the energy of the incoming ion beam to a few electronvolts at the entrance of the trap, i.e., $E = eU_i$ as illustrated in Fig. 1(b). The remaining energy is dissipated in the cooler buncher via room-temperature helium buffer gas cooling, laser cooling, or a combination of both. The ions are cooled into the bottom of the Paul-trap's potential well, which is in these studies typically $U_w \approx 7$ eV below the potential barrier at the trap entrance, shown in Fig. 1(b). Thus, a total energy of $E = e(U_i + U_w)$ has to be dissipated by the ion-cooling process before the equilibrium temperature is reached. Note that U_w in our application is of similar value to potential wells typically employed in cooler bunchers at RIB facilities.

A precision needle valve controls the flow of helium gas into the Paul trap to typical pressures ranging from a residual pressure of 10^{-8} mbar, when the valve is closed, to 10^{-5} mbar, as measured by a pressure gauge connected to the vacuum chamber housing the Paul trap. According to gas-flow simulations performed in Molflow+ [75], a helium pressure of 10^{-5} mbar in the vacuum chamber corresponds to 10^{-2} mbar inside the Paul trap, when helium is being leaked in.

When laser cooling is applied, a continuous-wave laser beam with a wavelength of 280 nm with typical laser powers of 0.25 to 20 mW and a diameter of 2 mm is directed into the Paul trap during the entire measurement sequence. Due to the lack of transversal optical access in the present setup, the laser direction is limited to the longitudinal axis of the Paul trap. For Doppler cooling, the frequency of the laser is set below the resonance frequency (i.e., red-detuned) of the $3s^2S_{1/2} \rightarrow 3p^2P_{3/2}$ transition (D2 line) of the singly charged Mg^+ ions. The addition of low-pressure buffer gas speeds up the initial ion-energy reduction from higher energies (>7 eV at the point of injection) to energies at which laser cooling can be efficiently applied.

The laser light used for Doppler cooling of Mg^+ ions is generated by the setup detailed in Ref. [65]. In short, a Spectra Physics 20 W Millennia eV laser (Nd-YAG) produces 532 nm laser light that pumps a Sirah MATISSE dye laser to create 560 nm output light. The latter is coupled into a high-power, large-mode-area 25-m-long optical fiber

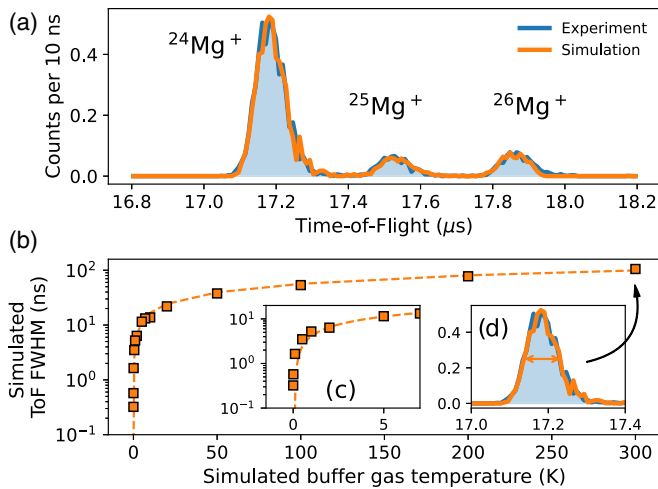


FIG. 2. (a) Time-of-flight spectrum of $^{24,25,26}\text{Mg}^+$ ions from ion optical simulations including 300 K buffer-gas cooling (orange) and experimental data (blue). The simulation is normalized in intensity to the experimental data. (b) Simulated FWHM values of time-of-flight spectra as a function of buffer-gas temperature fitted to a square-root function (dashed orange line). (c) shows a zoom of (b) at lower temperatures. (d) shows a zoom of (a), with additional arrows indicating the FWHM and corresponding data point.

for transport of the laser light from the laser room to the ion-trap laboratory. Here, the second-harmonic laser light at 280 nm is generated utilizing a SIRAH WaveTrain-2 frequency doubler. The output of the doubler is then focused and directed along the axis of the Paul trap cooler buncher, where the Doppler cooling takes place. The wavelength meter (HighFinesse ANGSTROM WS/U-10) used in the experiment was calibrated with a reference wavelength provided by a stabilized diode laser (Toptica DL PRO 780). The laser linewidth of ~ 1 MHz is small compared to the 41 MHz natural linewidth of the D2 line [43].

The Mg^+ ions are cooled for the full duration of the time they spend in the trap. As a result of the cooling process, the ions end up close to the axial potential minimum near the ejection side of the Paul trap. The ion bunch is subsequently ejected, accelerated to an energy of 2.2 keV and directed toward the MR-ToF device by a second 90° quadrupole bender. The ions are detected on one of two MagneTOF ion-ToF detectors, positioned in front and behind the MR-ToF device. While the ions are stored in the MR-ToF device [48], they perform up to several thousand revolutions, being reflected back and forth between two electrostatic mirrors. This increases their overall flight time, during which ions of different masses separate. The three outermost mirror electrodes are passively stabilized and the second outermost one is additionally actively stabilized to reduce fluctuations in the ions' ToF as described in Refs. [76,77]. A more detailed description of the operational principles of MR-ToF devices can be found in Refs. [48,78].

An example of a ToF spectrum obtained after room-temperature buffer-gas cooling without trapping in the MR-ToF instrument is shown in Fig. 2(a). The ions' ToF values are depicted with respect to the extraction trigger of the Paul trap. The experimental data is compared to ion-optical simulations

of the ion trajectories in the Paul trap and subsequent ion transport following the procedures explained in Ref. [66]. Overall, the simulations yield excellent agreement with the experimental data.

The full width at half maximum (FWHM) of the ToF spectrum after ion extraction from the Paul trap cooler buncher is indicative of the temperature of the ion ensemble in the trap and closely follows a square-root dependence on temperature [50,79]. This was reproduced in ion optical simulations: The reduction of the buffer-gas temperature results in a reduced FWHM of the ToF peaks following the expected trend, as shown in Fig 2(b). The FWHM of the ToF peak structures as measured on the ion detector is used in the following sections to compare buffer-gas and Doppler cooling.

III. EXPERIMENTAL RESULTS

The effectiveness of Doppler cooling in reducing the ion-ensemble temperature below those achievable by room-temperature buffer-gas cooling becomes apparent in Fig. 3. Here, the experimental ToF spectra are presented for three cases: (1) He buffer gas cooling at 300 K and 5×10^{-7} mbar as measured in the surrounding vacuum chamber (green). Ions were loaded into the trap for a 100- μs -long loading time and cooled for the duration of 500 ms, leading to a FWHM of the ToF spectrum of 100(8) ns. (2) Neither buffer-gas nor laser cooling of the ion bunch, with only the background residual gas present in the system at a pressure of 3×10^{-8} mbar (orange). Due to the reduced capture efficiency with respect to standard buffer-gas cooling, the loading time was adjusted to 10 ms. The FWHM after extraction of the ion bunches was 103(10) ns. (3) Doppler cooling with an on-axis laser of 6 mW in the presence of the background residual gas (blue), performed under the same conditions as for the residual-gas cooling data alone. In this case, the cooling laser was detuned by -150 MHz with respect to the D2 transition frequency in $^{24}\text{Mg}^+$ ions and applied for the full duration of the cooling

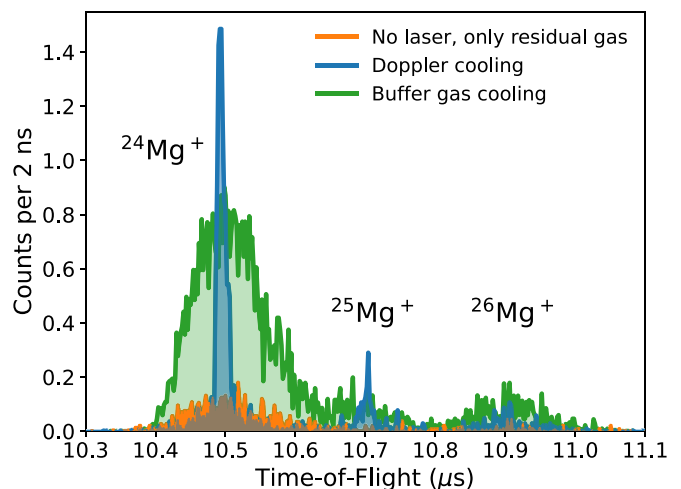


FIG. 3. Time-of-flight spectrum of $^{24,25,26}\text{Mg}^+$ ions after extraction from the Paul trap cooler-buncher as measured on the retractable ion detector in front of the MR-ToF device using Doppler cooling (blue), buffer-gas cooling (green), and residual gas cooling (orange).

time of 500 ms after injection as described in Sec. II. A reduction in FWHM from 100(8) ns for buffer-gas cooling to 12(1) ns for laser cooling is obtained for $^{24}\text{Mg}^+$ ions. According to the results of the ion-thermometry simulations in Fig. 2, a buffer gas of 6 K would be required to achieve a similar ToF width as obtained with Doppler cooling in this example.¹ In addition, ion-optical simulations show that, by optimizing the ion-acceleration section downstream of the Paul trap, a ToF spread of 4(1) ns would be achievable under the same experimental conditions for laser-cooled ion bunches. The time spread of buffer-gas cooled ions would barely be affected by these changes and, in the simulation, result in a ToF spread of 107(4) ns for the optimized acceleration potentials compared to 105(4) ns for the experimentally used ones.

A. Cooling systematics

The theoretical photon scattering rate of ions at rest for different detuning frequencies with respect to $^{24}\text{Mg}^+$ ions is shown in Fig. 4(a). For $^{24,25,26}\text{Mg}^+$ ions, the area of each peak is scaled to their natural abundance ratio and single-transition, angular-momentum coupling estimates of transition intensity (i.e., Racah transition intensities). The width of all peaks corresponds to the natural line width of 41 MHz [43]. The insert shows the relevant transitions for $^{24,26}\text{Mg}^+$ and $^{25}\text{Mg}^+$ ions in blue and orange colors, respectively.

Since Doppler cooling is based on red-detuning of the cooling laser from the transition frequency and all three stable isotope species of magnesium are co-trapped in the Paul trap cooler buncher during the cooling process, the isotope shift $\delta\nu^{A,A'} = \nu^{A'} - \nu^A$ between them determines that each isotope will experience a different frequency detuning. This implies that at a fixed laser frequency, the different isotopes show varying photon scattering and thus cooling rates. Additionally, the only stable magnesium isotope with nuclear spin $I \neq 0$ is ^{25}Mg ($I = 5/2$), where the hyperfine interaction gives rise to six hyperfine levels, as shown in the insert of Fig. 4(a).

By scanning the frequency detuning of the cooling laser, the effect of the differing cooling rates for $^{24,25,26}\text{Mg}^+$ ions becomes apparent, indicated by the width of the corresponding ToF signals shown in Fig. 4(b). The influence of increased laser power and cooling time are shown in Figs. 4(c) and 4(d), respectively. For all experimental results shown here, a residual gas pressure of $\approx 10^{-8}$ mbar was measured in the vacuum chamber.

From Fig. 4(c), it becomes apparent that an increased laser power for a fixed frequency and cooling time has a positive effect on the number of laser-cooled ions. At intermediate laser powers, we observe a distinct separation of laser-cooled ions, represented by a narrow ToF width on top of a wide ToF distribution due to hot ions. The latter is of similar

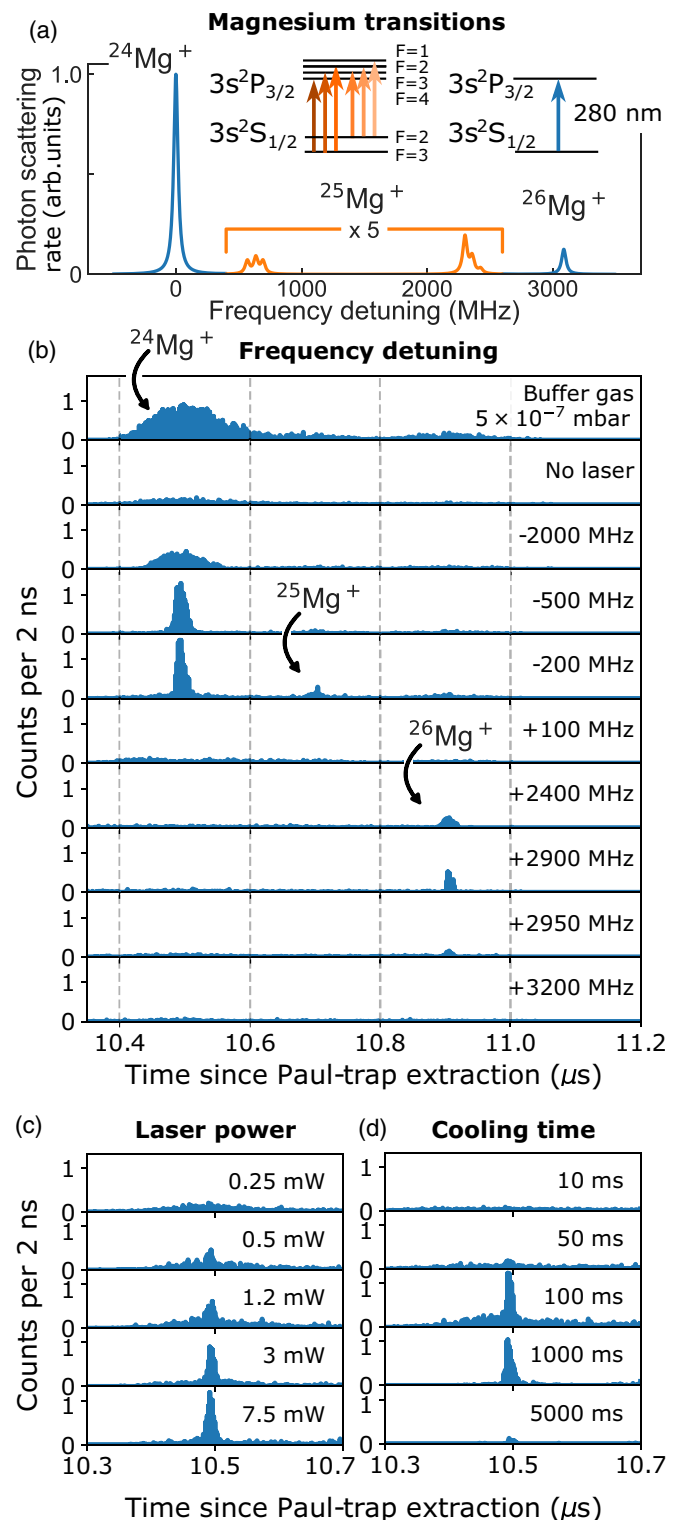


FIG. 4. (a) Photon-scattering rates calculated as a function of laser-frequency detuning from the D2 transition in $^{24}\text{Mg}^+$ ions. ToF spectra for laser-cooling systematics at residual gas pressures as a function of (b) laser detuning at 3 mW and 500 ms cooling, (c) laser power at 200 ms cooling and -200 MHz detuning, (d) cooling time at 3 mW and -200 MHz detuning, as measured on the first, retractable ion detector.

¹We note that the ion optical simulations indicate that the time-focus point for cooling at varying buffer-gas temperatures and laser-cooled ions occur at different spatial positions. Thus, the comparison of the ToF widths for different cooling schemes at a fixed detector position may provide an incomplete picture. In fact, the energy distribution of the simulated laser-cooled ions suggests that the (longitudinal) ion-cloud temperature is actually < 1 K.

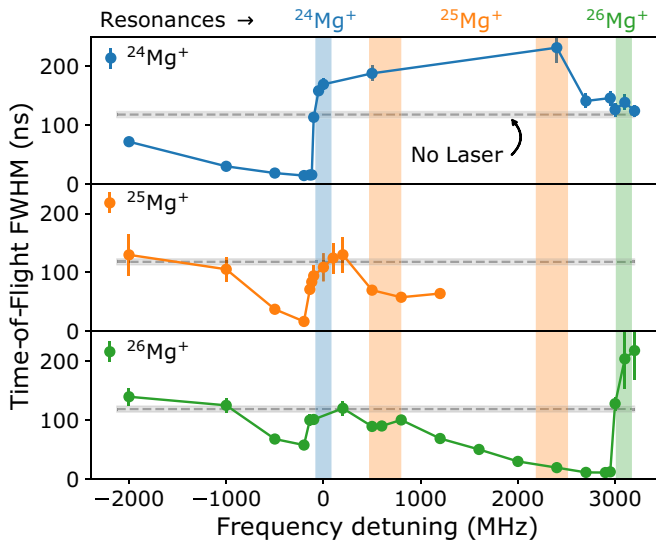


FIG. 5. FWHM of the time-of-flight spectra for $^{24,25,26}\text{Mg}^+$ ions as a function of laser-frequency detuning with respect to the D2 transition in $^{24}\text{Mg}^+$ ions. Resonance frequencies for $^{24,25,26}\text{Mg}^+$ are represented as colored bands.

width as in the case of buffer-gas or residual-gas cooling, which indicates that these ions have experienced only a few absorption-emission cycles, if any. When the laser power is increased from 0.25 mW to 7.5 mW, the total ion count rate stays nearly constant at 12 counts per bunch while the fraction of laser-cooled ions increases significantly from 1.6 to 7.5 counts per bunch. The cooling time variation shown in Fig. 4(d) shows similar behavior; laser cooled ions are first observed for cooling times as low as 50 ms. With increasing cooling time, the fraction of laser-cooled ions becomes larger while the background of noncooled ions decreases. Cooling longer than 1 s increases the overall ion losses, most likely due to collisions or charge exchange with residual gas atoms.

When the laser is red detuned with respect to the ion species' respective transition frequencies, Doppler cooling takes place and the FWHM of the ToF signal drops for each magnesium isotope. Trapped ions interacting with a blue detuned laser frequency experience heating. This effect is observed as a sudden increase of the FWHM in measured ToF signals to values larger than without laser-ion interaction. Both effects of laser cooling and heating are visible in Fig. 5, where the width of the ToF peaks extracted from Gaussian fits of the ToF spectrum is shown as a function of frequency detuning for each of the three magnesium isotopes.

The cooling effect is observed below the transition frequencies, indicated as vertical colored bands, as the FWHM sinks below the gray reference line, i.e., the ToF width without any laser beam present. The hyperfine splitting in the D2 transition in $^{25}\text{Mg}^+$ ions complicates the laser interaction with this isotope as the ion population is transferred between the two hyperfine levels of the $3s\ ^2S_{1/2}$ fine structure state. Hence, laser cooling can proceed exclusively with a single laser frequency if it is red detuned to all six transitions in the D2 line, albeit at a reduced cooling rate. This might (partially) explain the higher ToF width at frequencies close to the

lower-frequency multiplet compared to the other magnesium isotopes on their respective resonance frequencies.

The FWHM increase due to heating is visible in Fig. 5 when the laser frequency is varied from below to above the resonance frequency around 0 MHz and +3000 MHz for $^{24}\text{Mg}^+$ and $^{26}\text{Mg}^+$ ions respectively. Because of the shift in resonance frequency for different isotopes, a single laser frequency can be blue detuned for one species, but red detuned for another. It is thus possible for a laser to heat $^{24}\text{Mg}^+$ ions while cooling $^{25,26}\text{Mg}^+$ ions. This is the case for frequency values between 0 and +3000 MHz in Figs. 4(a) and 5. However, the cooling of $^{26}\text{Mg}^+$ ions is strong enough to overcome the interaction with the heated $^{24}\text{Mg}^+$ ions. This is seen from the reduced ToF FWHM values at detuning frequencies closer to the resonance frequency of $^{26}\text{Mg}^+$ ions, i.e., from +1000 MHz to +3000 MHz in Fig. 5. The data for $^{25}\text{Mg}^+$ are limited to the region up to 1200 MHz. Above that value, laser heating of $^{24}\text{Mg}^+$ ions leads to its signal overlapping with $^{25}\text{Mg}^+$ ions which prevents a reliable determination of the latter's ToF width.

Because of the simultaneous trapping of all magnesium isotopes, laser-heated $^{24}\text{Mg}^+$ ions may also influence the temperature of cotrapped $^{25,26}\text{Mg}^+$ ions through ion-ion interactions. In particular, a clear cooling feature for all isotopes is observed on the red-detuned side of the transition frequency of $^{24}\text{Mg}^+$ ions, likely indicating sympathetic cooling of $^{25,26}\text{Mg}^+$ ions induced by the more abundant $^{24}\text{Mg}^+$ ions. Indeed, the ToF width reduction in $^{25,26}\text{Mg}^+$ ions as shown in Fig. 5 is close to the one found for $^{24}\text{Mg}^+$ ions. This would not be expected for direct laser cooling of $^{25}\text{Mg}^+$ ions at this detuning frequency. Nevertheless, contributions due to direct laser cooling of $^{25,26}\text{Mg}^+$ ions at a less efficient cooling rate cannot be excluded.

B. Sympathetic cooling of K^+ and O_2^+ ions

Since Doppler cooling requires a closed level system, its applicability is limited to isotopes with a suitable ionic level structure. This would limit the technique to only a select number of ion species. As already indicated by the results of the previous section, this restriction can be overcome by sympathetic cooling, where cotrapped ion species are cooled down through interactions with laser-cooled trapped ions. Indications of sympathetic cooling of $^{25,26}\text{Mg}^+$ are present in Fig. 5. However, as pointed out above, we cannot exclude a potential contribution of direct Doppler cooling of $^{25,26}\text{Mg}^+$ ions. As demonstration of the sympathetic cooling technique in the present apparatus, either potassium K^+ ions or molecular oxygen ions O_2^+ were thus cotrapped with laser-cooled $^{24}\text{Mg}^+$ ions. For laser powers, cooling times, and buffer-gas pressures similar to those described above, we observe a clear increase in trapping and cooling efficiency of both co-trapped species as shown in Fig. 6.

As expected, the final temperature reduction for similar cooling times and laser powers is not as high as in the case of direct Doppler cooling. Nevertheless, we observe a reduction in ToF FWHM for $^{16}\text{O}_2^+$ ions from 113(5) to 58(4) ns and for $^{39}\text{K}^+$ ions from 180(13) to 145(5) ns. Additionally, the number of trapped ions per bunch increases by a factor of 2.6 for oxygen and a factor of 2 for potassium. In the present paper,

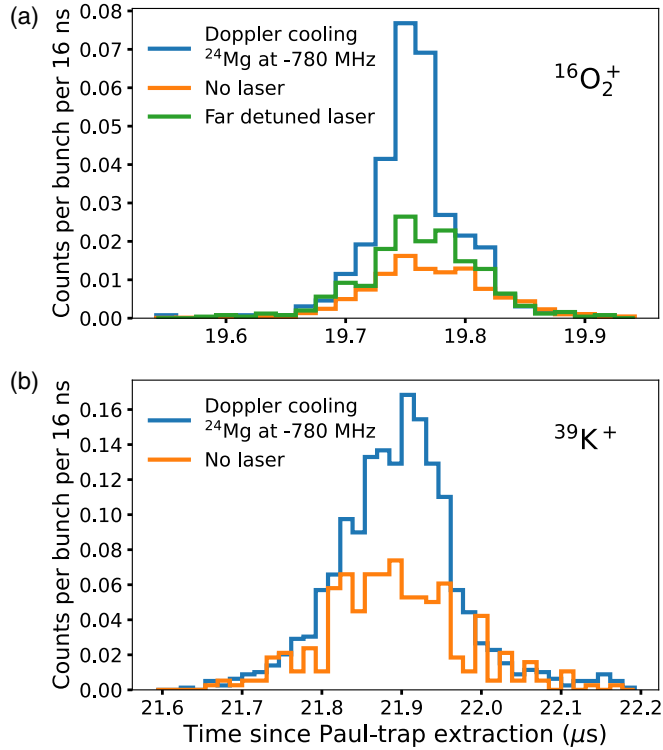


FIG. 6. Sympathetic cooling of molecular oxygen, $^{16}\text{O}_2^+$, and atomic potassium, $^{39}\text{K}^+$ ions. Sympathetic cooling of oxygen at 800 ms loading time and 600 ms cooling time with 20 mW of laser power. Same settings for potassium. See text for details.

sympathetic cooling experiments have been limited by reliable tuning of the intensity ratios of injected isotope species. With further improvements, sympathetic cooling performance similar to the results in more specialized work [80,81] can be expected. This way, ion temperatures approaching the one of the directly Doppler cooled ions are expected. Monitoring the cooling dynamics of the ions using a photon detector, not available in this work, could provide additional guidance in such a program. However, the present results already show that sympathetic cooling of atomic and molecular ions is applicable at RIB facilities.

IV. COOLING SIMULATIONS AND MODEL

A. Ion optical simulations

The trajectories of trapped magnesium ions are simulated using the ion-optical software package SIMION 8.2 [82]. The simulations include ion dynamics inside the Paul trap, subsequent ejection from the trap, and transport up to the ion detector, similarly to the implementation in Ref. [66]. To obtain an initial ion distribution for laser-cooling simulations, ions are first left to thermalize in a room-temperature buffer gas modeled by SIMION's hard-sphere interaction HS1 [83]. The ion ensemble obtained at the end of this simulation is then used as a starting point for further laser-cooling simulations, also performed with SIMION.

The laser-cooling simulation starts with the prethermalized magnesium ions already inside the cooler buncher. The effect of the laser-ion interaction on trapped-ion dynamics

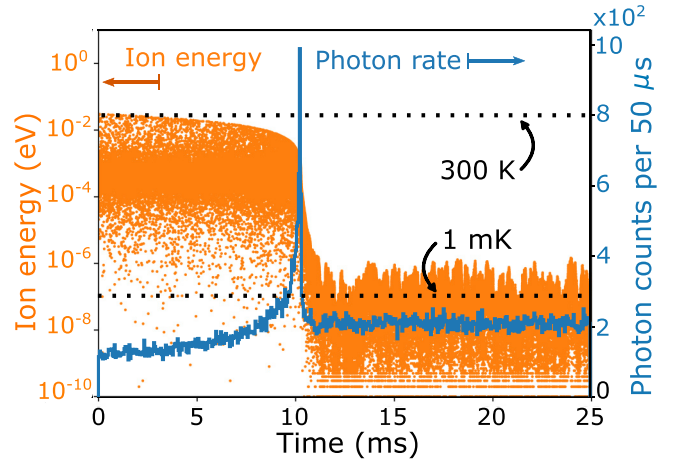


FIG. 7. Simulated energy for a single $^{24}\text{Mg}^+$ ion (orange) at each time when a photon-ion interaction takes place. The photon scattering rate per 50 μs (blue) is indicated on the right y axis. The simulation is performed for an ion with 0.03 eV initial energy being cooled by a 200 MHz red-detuned cooling laser with 25 mW power and 2 mm diameter.

is modeled in a semiclassical Monte Carlo manner. At each time step of the simulation, the ion's instantaneous velocity with respect to the laser-beam direction was used as an input parameter for a calculation of the Doppler-shifted frequency detuning from resonance Δ , i.e., the laser-frequency detuning from resonance as perceived by the ion, as well as the photon scattering rate [42],

$$\mathcal{R}(\Delta) = \frac{\Gamma}{2} \frac{I/I_{\text{sat}}}{1 + I/I_{\text{sat}} + 4\Delta^2/\Gamma^2}, \quad (2)$$

where Γ is the transition width, I is the laser power density, and

$$I_{\text{sat}} = \frac{\pi}{3} \frac{hc}{\lambda^3 \tau} \quad (3)$$

is the saturation power density of the transition, h represents Planck's constant, c the speed of light, the transition wavelength is given by λ and the lifetime $\tau = \Gamma^{-1}$ [42]. The calculated scattering rate is converted into a photon-ion interaction probability. A random number generator signals a photon event when the returned value is smaller than the interaction probability. In such an event, the photon momentum is subtracted from the magnesium ion momentum in the direction of the absorption. The momentum kick due to the re-emission of a photon is set to be prompt and in a random direction. Stimulated emission of photons is not taken into account.

An example of the result of the kinetic-energy evolution of a single trapped ion and photon scattering rate as a function of time are shown in Fig. 7. Here, an ion with initial energy of 0.03 eV interacts with a 25-mW and 2-mm diameter laser beam that is red detuned by -200 MHz in the absence of buffer gas. In Sec. VB 1, examples will be presented where buffer gas is included as well. Each point on the ion-energy scatter plot represents the ion energy at the time of interaction with a laser photon. The blue curve represents the instantaneous photon scattering rate. The largest drop in ion energy

takes place in a short time range when the overlap between ion energy and laser-frequency detuning matches. This coincides with a maximal photon scattering rate, seen as a distinct photopeak under the right cooling conditions.

B. Numerical cooling model

A second approach to describing the cooling dynamics models the energy evolution and photon scattering rate of a trapped ion being laser cooled in the presence of a buffer gas using a 1D numerical approach. Here, Doppler cooling of a single trapped ion in the weak binding regime [32], where Γ is larger than the oscillation frequency in the ion trap, is assumed [84] and buffer-gas cooling is added as an exponential decay term to the equation describing the ions energy evolution as a function of time [85]. The model applied in these simulations and the equations shown in this section were adopted from Refs. [84,85]. This 1D numerical model does not take into account any micromotion or RF-heating effects in the Paul trap, nor does it consider ion-ion interactions or stimulated emission effects.

The ion energy is determined by numerically solving a differential equation in reduced variables for ion energy E , frequency detuning Δ , and recoil energy $E_r = (\hbar k)^2/(2m)$ as $\{\varepsilon, \delta, r\} \equiv \{E, \hbar\Delta, E_r\}/E_0$, where $E_0 \equiv \hbar\Gamma\sqrt{(1+s_0)}/2$, and $\Gamma\sqrt{(1+s_0)}$ describes the power-broadened linewidth with the saturation parameter $s_0 = I/I_{\text{sat}}$. The variation of the reduced energy ε is described with respect to a reduced time $\mathcal{T} = t/t_0$, where t denotes time and $t_0 = (\frac{\Gamma}{2} \frac{s_0}{(1+s_0)})^{-1}$. The differential equation describing the energy evolution is given by

$$\frac{d\varepsilon}{d\mathcal{T}} = -\gamma(\varepsilon - \varepsilon_1) + \frac{4}{3}r \frac{1}{2\sqrt{\varepsilon r}} \text{Im}(Z) + \frac{1}{2\sqrt{\varepsilon r}} (\text{Re}(Z) + \delta \text{Im}(Z)), \quad (4)$$

with $Z = i\sqrt{1 - (\delta + i)^2/4\varepsilon r}$. The first term describes the buffer-gas interaction using the mobility γ [85,86] and the difference between instantaneous reduced energy ε and the reduced energy attainable by buffer gas cooling $\varepsilon_1 = k_B T/E_0$. The second term describes the stochastic recoil heating effect after photon emission, while the final term is used to model the laser-ion interaction. The fluorescence photon emission rate is given by

$$\frac{dN}{d\mathcal{T}} = \frac{1}{2\sqrt{\varepsilon r}} \text{Im}(Z). \quad (5)$$

The derivation of this equation is described in Appendix A of Ref. [84]. In contrast to Sec. IV A, where the laser-ion interaction was only included after room-temperature buffer-gas thermalization, Fig. 8 shows the energy evolution and photon scattering rate as a function of time for a $^{24}\text{Mg}^+$ ion with 10 eV initial energy being cooled simultaneously by a 300 K helium buffer gas at 1×10^{-5} mbar and a 200 MHz red-detuned cooling laser with 25 mW of laser power and 2 mm diameter. The mobility of magnesium ions in helium buffer gas is taken as $2.3 \times 10^{-3} \text{ m}^2 \text{ s}^{-1} \text{ V}^{-1}$ [85,87].

The initial cooling is dominated by the exponential buffer-gas cooling effect until the ion velocity distribution matches the laser detuning frequency and Doppler cooling becomes

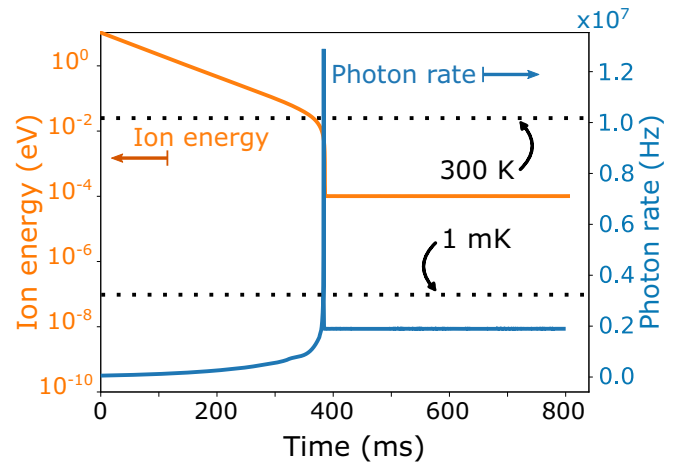


FIG. 8. Calculated energy for a single $^{24}\text{Mg}^+$ ion (orange) and instantaneous photon scattering rate (blue) as a function of time for an ion with 10 eV initial energy being cooled by a 300 K helium buffer gas at 10^{-5} mbar and a 200 MHz red-detuned cooling laser with 25 mW power and 2 mm diameter.

very efficient. This point is indicated by the photon fluorescence peak around 0.38 s in Fig. 8. This agrees well with the experimental data as shown in Fig. 4(d), where a significant fraction of the ions is cooled within 100 ms, considering the limited knowledge of the exact initial ion energies, buffer-gas pressure, and laser-ion overlap in experimental conditions. Under similar conditions, but in the absence of buffer gas, the photopeak would occur only after 137 s according to the numerical cooling model.

This indicates the importance of the background buffer gas in reducing the overall cooling time of the ion. The cooling times in the absence of a buffer gas would be prohibitively long for use at RIB facilities. The limit of 300 K in the case of buffer-gas cooling is indicated by the horizontal dashed lines in Figs. 7 and 8. The final energy reachable according to this numerical model is a balance between the buffer-gas and laser-cooling effects and depends on variables such as buffer-gas pressure, temperature, laser frequency detuning, and power density.

The findings in Refs. [84,85] show that laser cooling is most efficient when the laser-frequency detuning corresponds to half the width of the velocity distribution of the ions. As an alternative for speeding up the cooling process of hot trapped ions using low-pressure buffer gas, one could in principle use a fast-scanning laser that matches the ions' instantaneous velocity distribution [88]. With a fixed laser frequency and no added buffer gas, laser cooling of a 10-eV magnesium ion would take >100 s. However, according to the numerical cooling model, matching the laser-frequency at every moment in the cooling process would reduce this time down to <50 ms. This would require a laser with output power of 25 mW to chirp the laser frequency in a controlled manner over a range from -32 GHz detuning down to near 0 MHz detuning within 50 ms according to the time dependence as shown in Fig. 9. In this small time-step calculation, the frequency detuning was adjusted to the optimal one for the ion's instantaneous energy. This allows for a high photon scattering rate and strong ion-energy reduction during the full cooling time.

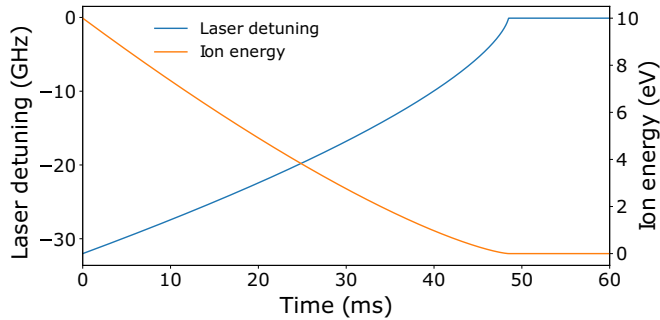


FIG. 9. Optimal laser-frequency detuning (blue) and corresponding ion energy (orange) as a function of time needed for cooling down a 10 eV $^{24}\text{Mg}^+$ ion in absence of a buffer gas as obtained from the 1D numerical model.

C. Comparison of both approaches

Results of the laser interaction introduced in ion-optical Monte Carlo simulations were benchmarked against the 1D numerical cooling model without buffer gas as shown in Fig. 10. In this comparison, the initial position and velocities of ions in the simulation were fixed to the axial direction of the Paul trap cooler buncher to reduce SIMION’s 3D model to 1D only. Both the ions’ kinetic energy, starting from 0.03 eV and the photon scattering rates are presented for different laser-frequency detuning settings. The agreement between the two methods, despite their different modeling, is excellent.

As can be seen from Fig. 10, the time needed for cooling the ions strongly depends on the laser frequency: The cooling efficiency for red-detuned laser frequencies depends on the photon-scattering probabilities over time. In the absence of a frequency-detuning, the ion energy remains unaffected [Fig. 10(a)]. Data in Figs. 10(b)–10(d) showing the laser-cooling effect of red-detuned laser frequencies of -20 , -200 ,

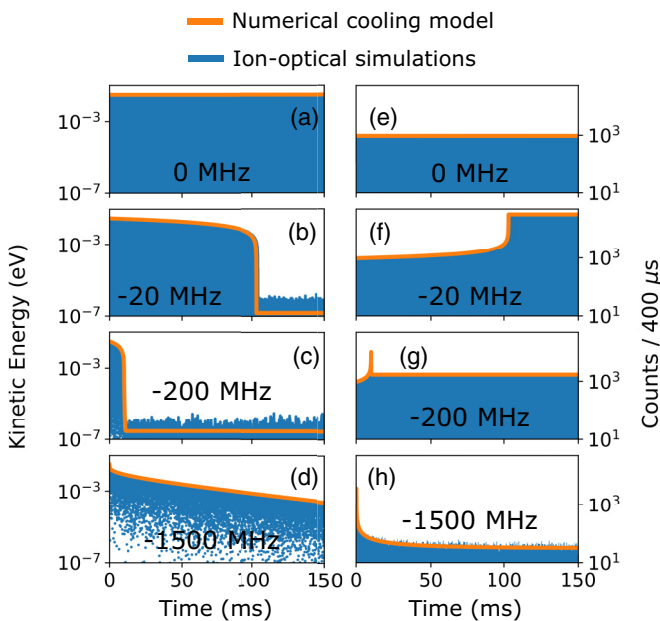


FIG. 10. (a)–(d) Kinetic energy and (e)–(h) scattered photon rate for the 1D numerical model (orange) and ion-optical simulations (blue) as a function of time for different laser detuning frequencies.

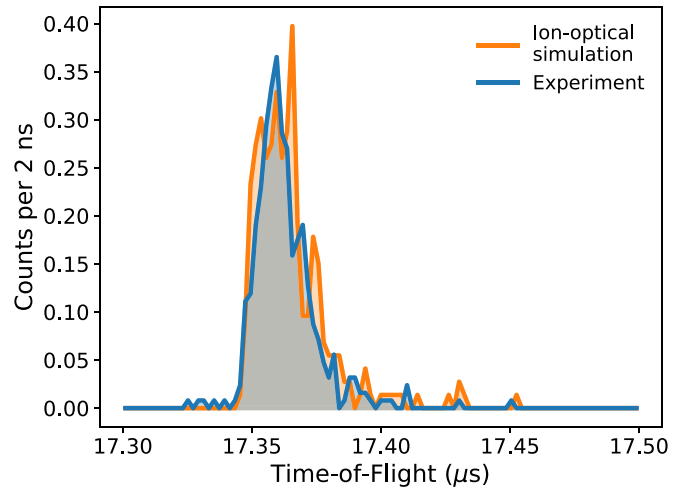


FIG. 11. Time-of-flight spectrum of Doppler-cooled $^{24}\text{Mg}^+$ ions. The experimental data are compared to ion-optical simulations. Both are obtained for a laser frequency detuning of -600 MHz with respect to the D2 transition, a laser power of 25 mW, and a cooling time of 150 ms. No residual gas is considered in the simulation. The only free simulation parameters are the ToF offset and the ion intensity, which were matched to experiment for better comparison.

and -1500 MHz indicate a significant cooling-time difference. This agrees with the experimental observations from Sec. III, where the laser-detuning frequency is identified as a key parameter for laser cooling efficiency.

D. Experimental benchmark of simulation and model

To evaluate the quality of the 3D ion-optical simulation, its results in terms of obtained ToF distributions are compared to experimental data. Under varying experimental conditions, ions are cooled, extracted from the Paul trap, and their flight time recorded at the position of the ion detector, see Fig. 1. Previous studies established good agreement between experiment and simulation when exclusively buffer-gas cooling is performed [66]. This conclusion is confirmed by the present paper, see for instance Fig. 2(a). An example of a ToF distribution for Doppler-cooled $^{24}\text{Mg}^+$ ions is shown in Fig. 11. The simulated data reproduces the shape and width of the experimental ToF peak, including a tail toward longer times. This provides evidence for the validity of our simulation approach when also considering the laser-ion interactions.

A more comprehensive comparison is given in Fig. 12. It summarizes the obtained FWHM of ToF spectra such as the one shown in Fig. 11 when varying the laser frequency detuning. Here, the experimental data are compared to results of (a) the numerical cooling model and (b) ion-optical simulations, where the effect of buffer-gas and laser cooling are simultaneously included for both. To reduce the computation time, both approaches start from room-temperature ions that are subsequently cooled by a laser with a saturation parameter $s_0 = 3.27$ for the duration of 150 ms. This differs from experiment, where the ions are injected into the cooler buncher with an estimated initial energy of >7 eV and are cooled for 600 ms. Note that, in the simulation, the exact cooling time has no influence on the results, provided that the equilibrium state

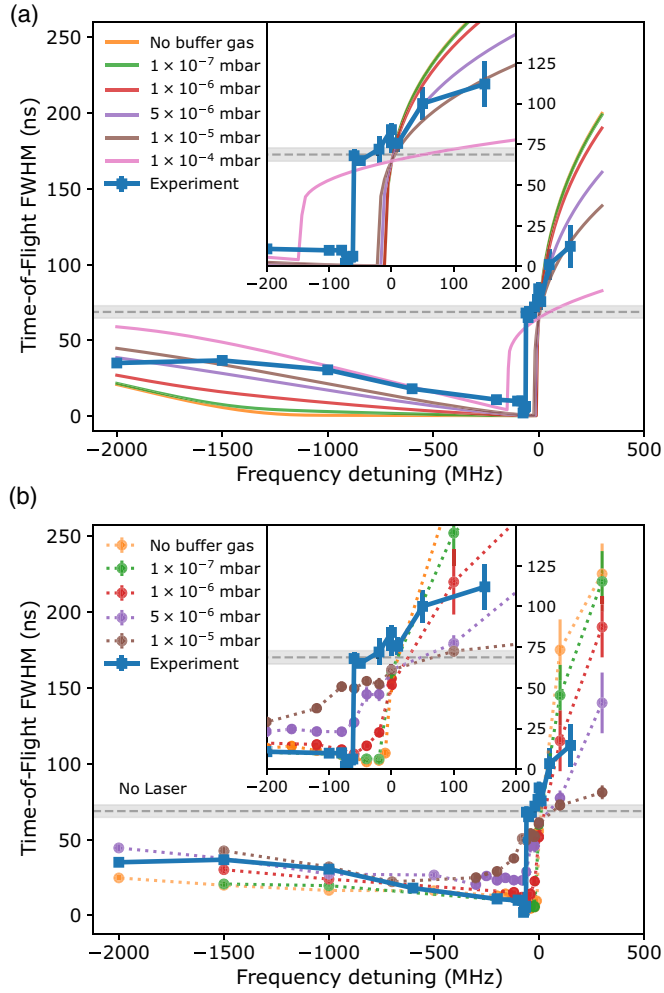


FIG. 12. Width of the experimental ToF signal of $^{24}\text{Mg}^+$ ions as a function of the cooling-laser frequency at a residual buffer-gas pressure of 1×10^{-8} mbar. Experimental data are shown as blue squares. Results from (a) the numerical model described in Sec. IV B and (b) ion-optical simulations described in Sec. IV A for different buffer-gas pressures. To obtain (a), the ion temperature obtained from the 1D Model is translated into a ToF width by employing the found relationship of Fig. 2(b). For reference, the experimental ToF width without injecting the laser beam into the Paul trap is shown as a grey band.

has been reached. This can also be seen in Figs. 7 and 8, where the ion energy remains constant once the cooling equilibrium is obtained.

As indicated in Fig. 12, the results of the 1D model and 3D simulation qualitatively agree with the experiment over the entire frequency range. As the most prominent feature in the data, a strong increase in the FWHM of the ToF signals the change from laser cooling to laser heating. This effect is clearly visible in the experimental data as well as in the 1D model and 3D simulation when low residual gas pressures are used. If the laser frequency matches the transition frequency of the D2 line exactly, the laser has no net effect on the ion energy [Figs. 10(a) and 10(e)]. Thus, at this frequency, all curves in Fig. 12(c) cross the grey band which represents the experimental ToF width for room-temperature buffer-gas

cooling without a laser injected into the Paul trap. This is also the case for the experimental data, but the sharp increase in the ToF width is shifted by a few tens of megahertz to red-detuned laser frequencies, see inserts of Fig. 12. This is attributed to potentially two reasons. First, the accuracy of the employed wavelength meter for the 560 nm fundamental laser light is 30 MHz, given the used calibration wavelength. This leads to a 60 MHz uncertainty on the absolute frequency of the cooling laser. Second, incomplete ion cooling before reaching equilibrium or the presence of residual gas smear out the otherwise sharp cooling-heating transition. The latter effect can be seen in both the 1D model as well as the 3D simulation for pressures exceeding $\sim 1 \times 10^{-5}$ mbar, although the exact shape of this transition differs slightly in the two methods.

More generally, the buffer-gas interactions reduce the effect of the laser-cooling. This is also visible on the red-detuned, laser-cooling side. It results in a higher ToF FWHM when buffer-gas interactions are included in simulations and the opposite effect is present for a blue-detuned laser frequency. Far from the transition frequency, where the relative importance of buffer-gas cooling is the largest, 3D ion-optical simulations agree better with experimental findings than the 1D numerical model. This is likely due to the more accurate implementation of buffer-gas cooling by use of the hard-sphere modeling.

In summary, both the 1D model and 3D simulations reproduce the experimental ToF data, which indicates that the relevant cooling physics is well captured. This provides confidence that other ion-bunch properties, not accessible in experiment, can be reliably studied by means of the developed cooling models. Moreover, the same tools can be employed to evaluate the implications of laser cooling of RIBs for specific experiments.

V. EXPERIMENTAL APPLICATIONS

The technique for cooling an ion ensemble using a combination of low-pressure background gas and laser cooling as presented here is beneficial for many RIB applications. Such applications using short-lived radioactive ions include, for instance, trapping and laser or sympathetic cooling for high precision spectroscopy, (collinear) laser spectroscopy on atomic and molecular ions, or mass measurements.

A. Mass spectrometry

1. Demonstration of an improved mass-resolving power in a multireflection time-of-flight device

To demonstrate the improved beam emittance and the potential use for mass measurements at RIB facilities, Doppler-cooled ion bunches are injected into a 1.5-keV MR-ToF device [65–69] and the mass-resolving power after laser cooling is compared with buffer-gas and residual-gas cooled ions. To this end, the mass-resolving power R is investigated as a function of storage duration in the MR-ToF spectrometer. The obtained data shown in Fig. 13 is compared to a fit using the following equation:

$$R_{N_a} = \frac{m}{\Delta m} = \frac{t}{2\Delta t} = \frac{t_0/N_a + t_a}{2\sqrt{\Delta t_a^2 + (\Delta t_0/N_a)^2}}, \quad (6)$$

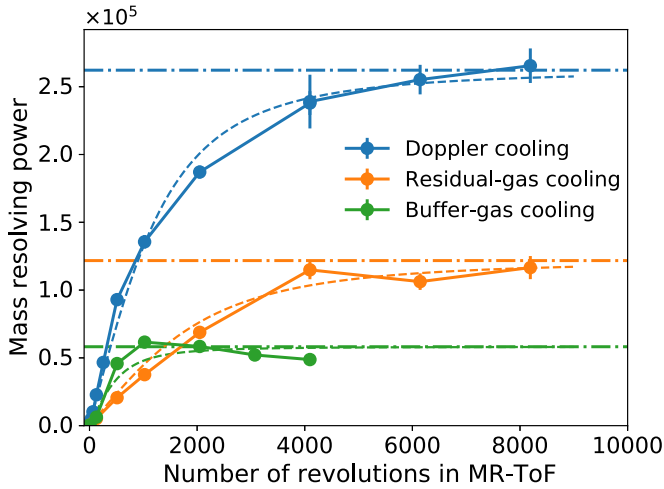


FIG. 13. Mass resolving power for the $^{24}\text{Mg}^+$ ion signal as a function of storage time in the MR-ToF device for three different cooling mechanisms. Solid lines are fits of Eq.(6) to the data. Dashed lines denote the saturation resolving power R_∞ .

describing the mass-resolving power in an MR-ToF spectrometer [50]. Here N_a is the number of turns in the MR-ToF instrument and $t_0 = 17.35 \mu\text{s}$ represents the time it takes for the ions to reach the ToF detector without trapping in the MR-ToF device. Δt_0 denotes the FWHM of the ToF signal due to initial conditions (20 ns for laser cooling and 80 ns for buffer- and residual gas cooling) and $t_a = 6.7 \mu\text{s}$ the period of a single revolution in the spectrometer, which are both measured. Δt_a describes the increment in ToF-distribution width induced during each period due to aberrations and was left as the only free fitting parameter.

For Doppler-cooled magnesium ions, an improvement of a factor 4.6 in mass-resolving power R_∞ from 57 000 for standard buffer-gas cooled ions to 261 000 was observed. A mass-resolving power of 50 000 is reached after 250 revolutions for laser cooling, which is five times faster than for residual gas cooling and 2.6 times faster than for standard buffer-gas cooling. We note in passing that the present limit of the mass-resolving power for buffer-gas cooled ions seems to be due to collisions between ions and residual gas in the MR-ToF device: Adding buffer gas in the cooler buncher increases the pressure in the MR-ToF region as well, where collisions increase beam losses, very similar to the effects described in Ref. [89]. Therefore, the mass-resolving power can only be determined up to about 30 ms of storage time, corresponding to roughly 4500 revolutions in the MR-ToF mass spectrometer. Additionally, if the cooling in the Paul trap is only due to collisions with residual-gas atoms, the pressure in the MR-ToF device is lower, and hence larger mass-resolving powers can be reached than for standard buffer gas cooling. The resolving power obtained for residual-gas cooled ions is $R_\infty = 125\,000$. An adverse effect, on the other hand, is that the storage efficiency of magnesium ions in the Paul trap is strongly reduced for residual-gas cooling as compared with buffer-gas and Doppler cooling.

The ToF spread of an ion bunch in an MR-ToF device not only relies on the temperature of the ion ensemble but can also be affected by other variables such as the strength of

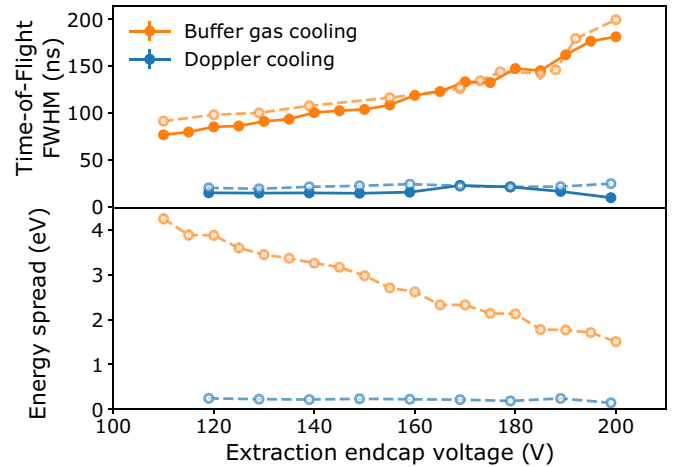


FIG. 14. Simulation (dashed) and experimental (full) ToF and energy-spread results for varying Paul-trap extraction field strengths of Doppler and buffer-gas cooled ions. Both observables are evaluated at the ion-detector position without trapping in the MR-ToF device.

the electric field used for extraction from the Paul trap [90] or whether the MR-ToF instrument is operated in a so-called isochronous mode [91]. In this mode, the MR-ToF electrode potentials are tuned to minimize the ToF dependence on ion energy. The measurements shown here were all performed in isochronous operation and using the same Paul-trap extraction field of about 2 V/mm.

We note that when minimizing the ToF spread by varying the extraction field from the Paul trap, a trade-off happens between ToF- and energy spread as emittance remains conserved. This is confirmed in the ion-optical simulations shown in Fig. 14. There it is shown that a reduction in ToF peak width by variation of the extraction field significantly increases the energy spread of the ions. Once the energy spread is too large and stretches beyond the isochronous region of the MR-ToF operation, the resulting mass-resolving power is eventually decreased.

The central advantage of laser cooling for MR-ToF mass spectrometry is that both the ToF and energy spread of the ion bunch are strongly diminished at the same time. Figure 14 illustrates the significant improvement in both ion-bunch properties by laser cooling over buffer gas. Once again, the experimental data on the ToF width are well reproduced by ion-optical simulation. Recalling that the longitudinal emittance equals to $\Delta E \Delta t$ at the time-focus point, it is a consequence of the reduced overall ion-beam emittance facilitated by laser cooling which enables an improved MR-ToF performance as compared to standard room-temperature buffer gas.

2. Impact on phase-imaging-based Penning-trap mass spectrometry

Penning trap mass spectrometry is currently the most precise and accurate approach to determine the mass of charged particles, stable or radioactive [92]. It is based on the measurement of the cyclotron frequency of an ion confined in a strong and uniform magnetic field. Among the techniques

available for cyclotron frequency determination, the PI-ICR technique [52] provides a superior resolving power and precision compared to other techniques under typical experimental conditions. In essence, PI-ICR relies on measuring the phase evolution of an ion's motion inside the Penning trap. The ion is ejected from the Penning trap onto a position-sensitive detector, which enables the reconstruction of the phase of the motion and, thus, its cyclotron frequency. Accordingly, the mass-resolving power is directly proportional to the spatial spread of the ions hitting the detector [92]. Therefore, by reducing the ion beam's radial spread, the application of novel beam preparation and cooling techniques has the potential to greatly impact the precision and resolving power obtained through PI-ICR.

To verify the conceivable impact of the techniques described in this paper to PI-ICR measurements, we perform simulations of a hypothetical PI-ICR procedure where $^{24}\text{Mg}^+$ ions are isotropically cooled to a given temperature inside the Paul trap employed in this experiment. The ions are sent to a Penning trap, where they are captured, accumulate a phase for a fixed amount of time, and are subsequently released toward a detector, where their spatial distribution is recorded. The Penning trap is modeled after the measurement Penning trap, operated by the TITAN Collaboration at TRIUMF [93], whose preceding simulations for employing the PI-ICR technique are described in Ref. [94]. The injection into the Penning trap is optimized for best trapping efficiency using an ion cloud of $T = 300$ K as reference, and an analysis of the spatial distribution of ions hitting the detector is performed with several beam temperatures down to 1 mK, the Doppler limit for cooling $^{24}\text{Mg}^+$ ions using the D2 line. It is important to note that PI-ICR's performance is highly reliant on the transversal emittance of the beam. Therefore, unlike the strictly longitudinal cooling performed in the experiment described in this paper, PI-ICR requires such cooling to be performed in all dimensions.

The results of the simulations are presented in Fig. 15. Overall, the FWHM of the detected beam image is proportional to the square root of the beam temperature. At 300 K, our simulations yield a beam spot FWHM of 1.75 mm, similarly as observed in well-established PI-ICR systems [52,95]. At sub-Kelvin temperatures, the beam spot FWHM is reduced by more than one order of magnitude, down to 220 times at 1 mK, which translates to a similar improvement in precision ($\delta m/m$), not having considered possible systematic effects. The improvement in mass precision and resolving power in a PI-ICR measurement should scale accordingly until other uncertainty contributions become equally or more relevant, such as the detector's spatial resolution, and imperfections and instabilities of the ion extraction field.

B. Laser spectroscopy

1. Demonstration of isotope shift measurements through observation of laser cooling-heating transition in time-of-flight measurements

The abrupt transition from laser cooling to laser heating takes place at the resonance frequency that corresponds to the isotope-dependent energy difference between the two involved electronic states. In our paper, this transition from

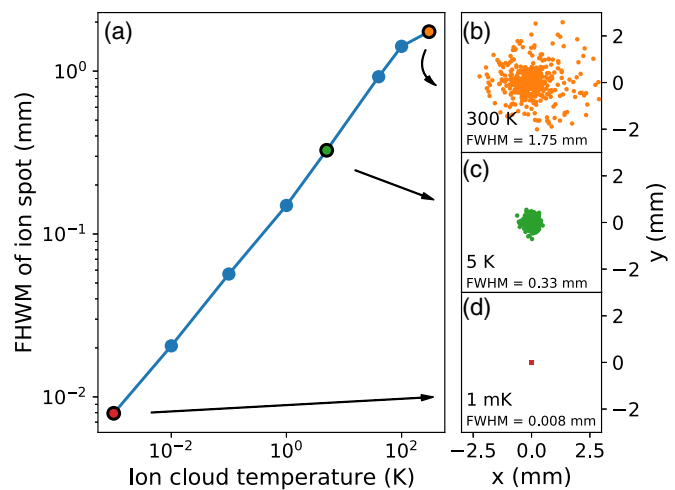


FIG. 15. (a) The spatial FWHM of the detected beam image after extraction from the Penning trap, as a function of beam temperature. In comparison to room temperature beam preparation, sub-Kelvin beam temperatures can yield an improvement in the precision of a PI-ICR measurement of well over an order of magnitude. (b)–(d) Example of simulated ion beam spots on the detector for three different ion cloud temperatures with their respective beam-spot sizes.

cooling to heating is visible as a steep increase in ToF width as seen in Figs. 5 and 12. This abrupt change in ToF width can thus be used to determine the resonance frequency and, consequently, also isotope shifts between different magnesium isotopes with nuclear spin $I = 0$. Unlike conventional isotope-shift measurements, this method does not require photon detection or extra laser steps for photoionization [47]. This method relies on the laser-frequency-dependent effect of Doppler cooling on the trapped ion momentum distribution, and probing that distribution through ToF measurements.

A scan of the cooling-laser frequency over cooling and heating transitions of both $^{24}\text{Mg}^+$ and $^{26}\text{Mg}^+$ ions is shown in Fig. 16. The sudden rises in FWHM are marked as the positions of the respective resonance frequencies. Their frequency difference corresponds to the isotope shift between the two nuclides.

The isotope shift extracted from this measurement, $\delta\nu^{26,24} = 3090(4)_{\text{stat}}\{26\}_{\text{sys}}$ MHz, is in good agreement with the literature value $\delta\nu_{\text{lit}}^{26,24} = 3087.560(87)$ MHz, obtained from a high-precision spectroscopy experiment [96], and our value is comparable in precision to collinear laser spectroscopy with fast ion beams at RIB facilities.

The systematic error quoted in our result stems from two contributions. First, the (relative) accuracy of the employed wavelength meter to which we have assigned a systematic uncertainty of 20 MHz in isotope shifts between Mg^+ ions following Ref. [68]. Second, it also stems from the pressure and mass-dependent offset of the cooling-to-heating transition from the absolute transition frequency. As discussed in Sec. IV D and shown in Fig. 12, the ion-optical simulations and the numerical model both predict a small pressure-dependent shift in the transition from cooling to heating. Our calculations confirm that this shift is very similar for isotopes that are close in mass and are measured in the same pressure conditions, as is the case for the current experiment.

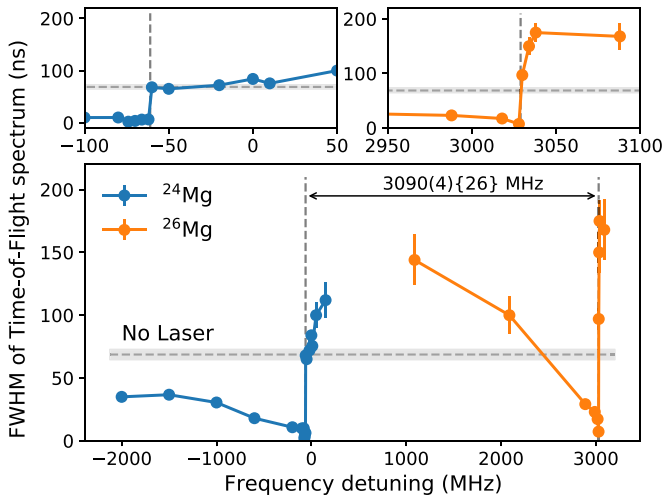


FIG. 16. Width of the experimental ToF signal as a function of the cooling-laser frequency, spanning laser cooling and heating of $^{24}\text{Mg}^+$ and $^{26}\text{Mg}^+$ ions. The x -axis offset is taken as the literature value for the absolute frequency of the D_2 ($3s^2S_{1/2} \rightarrow 3p^2P_{3/2}$) transition in $^{24}\text{Mg}^+$ ions, $\nu_{24} = 1\,072\,082\,934.33(16)$ MHz [96]. Two insets on top show a zoom in near the regions of interest of the data shown in the bottom part.

For isotopes that have larger mass differences, a systematic shift might occur due to different mass- and pressure-dependent cooling dynamics. The quoted systematic error contribution was estimated from the numerical cooling model, which returns the largest shift. For example, according to this model, a difference of 10 MHz from the actual isotope shift is expected between ^{20}Mg and ^{34}Mg at a pressure of 10^{-5} mbar (initial energy 10 eV, $s_0 = 3.27$, and 600 ms cooling). The shift between ^{24}Mg and ^{26}Mg remains within 16 MHz over the whole pressure range from 10^{-6} mbar to 10^{-4} mbar. Therefore, we estimate the systematic uncertainty due to the pressure and mass-dependent offset as such. The total systematic error adds up to 26 MHz.

Both the numerical cooling model and ion optical simulations shown in Fig. 12 suggest that the systematic error on the transition frequency and isotope shift determination could be reduced in future experiments by performing laser scans at different background pressures, since the different FWHM curves would cross at the resonance frequency when the cooling equilibrium is reached. Moreover, the systematic uncertainty due to the wavemeter can be decreased to a few megahertz by employing high-end models characterized in Refs. [97,98]. This technique can in principle be applied in online RIB conditions for all laser-coolable ions with sufficiently long half-lives to reach the cooling equilibrium. Some examples include the isotopic chains of Be, Mg, Ca, Sr, Ba, Ra, Hg, Yb, and Cd, that can either be laser cooled by a single laser or with the addition of a second repumping laser. The physics interest in these isotopic chains ranges from studying exotic nuclear shapes such as halo-nuclei [99] and the shell evolution [100–104] to King-plot nonlinearities and physics beyond the standard model [105]. If we focus on the case of ^{98}Cd , for instance, a 10-eV ion would be cooled in 800 ms in a 10^{-5} mbar helium buffer gas by a 214 nm laser of 2 mW laser power and 2 mm beam diameter. This cooling time is

significantly shorter than the 9.2(3) s half-life. Taking into account standard RIB efficiencies and a yield of 10 ions/ μC [106], such an experiment is feasible. For isotopes of these elements with very short half-lives ($\lesssim 500$ ms) and low yields, other approaches such as the MIRACLS technique of performing collinear laser spectroscopy in a 30-keV MR-ToF device [65,66,68] or the CRIS technique of collinear laser ionization spectroscopy [107] are better-suited high-resolution techniques.

2. Collinear laser spectroscopy

Collinear laser spectroscopy is a leading technique for precision laser spectroscopy at RIB facilities [46,108]. In this method, a narrow-band laser beam is overlapped with a fast ion beam. Counting emitted photons from laser-excited atoms or ions as a function of the laser frequency reveals the hyperfine structure of the studied transition and nuclide. The typically used ion beam energy of 30 to 60 keV results in a velocity compression which minimizes the Doppler broadening $\delta\nu$ due to the ions' energy spread δE according to $\delta\nu \propto \delta E/\sqrt{E}$ [109].

Modern applications of the technique employ cooler bunchers to accumulate and bunch the ion beam before the ions are sent into the laser spectroscopy beamline. This allows for a significant suppression of the photon background due to laser-stray light and detector dark counts by several orders of magnitude when gating the photon counting on the ion bunch's passage through the ion-laser-interaction and optical-detection region. Usual time spreads of ion bunches at RIB facilities are on the order of several microseconds [110].

As shown by our results, this can be readily reduced down to several nanoseconds when employing laser and sympathetic cooling in the cooler buncher. The ion bunch's significantly smaller temporal width, while maintaining a low-energy spread, will allow for an enhanced sensitivity by a factor of $O(10^3)$, narrowing the time-gating of ions passing through the optical-detection region. In practice, this will work best with axially segmented detection regions. Then, the flight time through a single segment is of similar order as the temporal bunch width itself while the cumulative laser-interaction and detection time remains of similar order as in contemporary CLS applications. Additionally, collinear laser spectroscopy could also benefit from an improved transverse emittance of a 3D-laser-cooled ion beam. This would maximize the overlap of the spectroscopy laser and the ion bunch and could improve the experimental sensitivity further.

C. Optimal future laser-cooling setup

While many of the proposed applications can be directly implemented in cooler bunchers which are operational in today's RIB facilities, the cooling performance could be fully optimized in a dedicated ion-trap system. Based on the proof-of-principle results from this Paul trap cooler-buncher, we propose a potential future device for delivering low-emittance bunched beams of radioactive ions. In the small Paul trap used in this experiment, the trapping efficiency during injection was significantly reduced when only residual buffer gas was present in the trap. Most likely, this was caused by insufficient cooling during the initial injection into and first oscillations

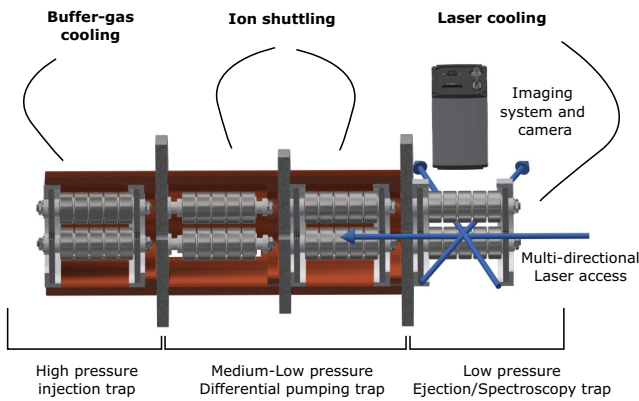


FIG. 17. Sketch of a future proposed cooler-buncher design for delivering low-emittance ion bunches and performing laser spectroscopy.

in the trap, causing a significant fraction of the injected ions to be lost at the start of the cooling cycle. Additionally, the combination of buffer gas and laser cooling in the same Paul trap speeds up the cooling with respect to laser cooling alone, but the presence of buffer gas also limits the achievable temperature. This would be undesired and even detrimental for experiments with cold trapped ions. Therefore, a future optimized setup should extend further in the axial direction and consist of several separate stages for cooling, where the buffer gas cooling is used primarily for initial cooling after which the ions are transmitted to a low-pressure Paul trap for subsequent laser cooling.

The envisioned cooler buncher, shown in a conceptual sketch in Fig. 17, would therefore consist of three segmented Paul-trap sections: a higher-pressure buffer gas cooling section, a two-stage differential pumping trap for ion shuttling at intermediate buffer-gas pressures, and, finally, a buffer-gas-free Paul trap dedicated to laser- and sympathetic cooling to achieve the low temperatures desired. The final section includes a photodetector for *in situ* monitoring of the cooling dynamics through detection of scattered photons. This will also allow this section of the device to be used for dedicated laser-spectroscopy studies using cold, trapped radioactive ions. These demands require the final stage trap to have an open structure with photon detection and multi-axis laser access, e.g., for laser cooling in all three dimensions. Additionally, the last stage has to be equipped with an ion source of stable, laser-coolable isotopes of different masses for sympathetic cooling purposes of a broad range of co-trapped ion species. An ion crystal of stable ions can then be formed before short-lived radioactive ions are injected for sympathetic cooling, similar as is done for stable (highly-charged) ions [111,112]. These short-lived ions would at this point have gone through the previous buffer-gas cooling stage. This proposed trap spatially separates the buffer gas and laser cooling, using different trap sections. An alternative approach might be considered where buffer gas and laser cooling happen in the same trap, but are separated temporally rather than spatially. Here, a burst of buffer gas fills the trap for a short time during injection of the ions. Subsequently, the buffer gas dissipates from the the trap, which allows laser

cooling to take place at low gas pressures. Such a burst of gas could be controlled using a piezo-actuated valve. A similar development as the latter proposal has been successfully achieved in Ref. [113], albeit at a timescale of 30 s to reach 3×10^{-11} mbar.

Experiments on cold trapped ions using radioactive species are of potential use for standard-model tests, fifth force, and dark matter candidate searches as well as for nuclear structure physics [57,63,64]. Realizing a setup as described above would form a first step toward such studies with short-lived radioactive isotopes at RIB facilities.

VI. CONCLUSIONS

We have introduced and studied, by corresponding experiments and calculations, the cooling of initially hot RIBs to sub-K temperatures, making use of laser- and sympathetic cooling in a cooler buncher in the presence of a low-pressure background gas. This technique was demonstrated to be fast enough for experiments with short-lived isotopes and can be readily implemented in current devices at RIB facilities. By use of these techniques, an improved beam emittance of Doppler-cooled magnesium and sympathetically cooled molecular oxygen and potassium ions was achieved. By combining Doppler cooling with a low-pressure helium background gas, the cooling time for ions with initial energies of at least 7 eV is reduced to suitable timescales for experiments at RIB facilities. Based on the reduction in ToF spread after extraction from a Paul trap cooler buncher, we estimate a temperature reduction factor of at least 50 after 200 ms of cooling, using ion-thermometry techniques. Additionally, our simulations show that this could be improved even further.

The improved ion bunch properties were further demonstrated by measuring an enhanced mass resolving power in an MR-ToF device. The experimental results were in good agreement with simulations performed in parallel, which in turn can guide future applications and improvements. As such, it was shown that the mass-resolving power in PI-ICR mass measurements could potentially be improved by up to two orders of magnitude. Other RIB experiments, such as (collinear) laser spectroscopy are also expected to significantly benefit from the improved ion beam emittance. Furthermore, it was shown that this technique can also be used for measuring isotope shifts of Doppler-coolable ions without the need for photon detection or additional laser steps for ionization.

Overall, the present results open possibilities for future high-precision experiments with cold trapped ions and significantly improved beam emittance at RIB facilities. By means of sympathetic cooling with co-trapped laser-coolable ions, this approach is universally applicable in providing cold ion samples and beams to subsequent RIB experiments. This includes sympathetic cooling of radioactive molecules which have recently been introduced as attractive new probes for searches of new physics [10].

As demonstrated in the present paper, the techniques can be readily implemented in existing instrumentation at RIB facilities. This will be the focus of our work in the near future. Ultimately, we envision a dedicated ion trap for laser and sympathetic cooling in all mass ranges which, in addition to its function as a next-generation RIB cooler buncher, could serve

as a platform for high-precision studies for nuclear structure and fundamental symmetries with trapped, radioactive ions.

ACKNOWLEDGMENTS

The research leading to these results has received funding from the European Research Council (ERC) under the European Unions Horizon 2020 research and innovation program under Grant Agreement No. 679038. Part of the work of S. Sels has been funded by Interne Fondsen KU Leuven/Internal Funds KU Leuven. The work of F. Maier has been sponsored by the Wolfgang Gentner Programme of the German Federal Ministry of Education and Research. P. F. and L.S. acknowledge support by the German Ministry for Education and Research (BMBF, No. 05P18HGCI A and No. 05P21HGCI1). R.N.W. acknowledges support by the Australian Research Council under the Discovery Early Career Researcher Award scheme (Award No. DE190101137). E.M.L and A.A.K. acknowledge support from the Natural Sciences and Engineering Research Council of Canada and the National Research Council of Canada through TRIUMF. M.A. acknowledges support from the European Union Horizon 2020 Research and Innovation Program under Grant Agreement No. 861198 project LISA (Laser Ionization and Spectroscopy of Actinides) Marie Skłodowska-Curie Innovative Training Network (ITN). We are thankful to W. Nörtershäuser and M. Mougeot for fruitful discussions and input to the paper. We are grateful for the support of the ISOLTRAP, COLLAPS, and RILIS collaborations at ISOLDE and, in particular, M. Mougeot, K. Crysallidis, and S. Wilkins for providing essential equipment and help. We

thank the CRIS collaboration for providing the diode laser for laser wavelength calibration, in particular, A. Koszorus and A. Vernon.

S.S. and S.M.-E. conceived the measurement idea following discussions with T.M. The experimental characterization of laser and buffer-gas cooling were conducted by S.S. and F.M., who also carried out the MR-ToF measurements together with C.K. Sympathetic cooling of other ion species was performed by F.M. and C.K. M.A. participated in a set of measurements utilizing buffer-gas cooling. The initial setup combining a Paul trap and an MR-ToF mass spectrometer has been built by R.W., P.F., and L.S. It was modified for laser applications by V.L., F.M., and S.M.-E. with contributions from P.F., S.L., P.P., and S.S. The potassium ion source and injection beamline was conceived and setup by D.L. and S.R. who coupled it to the ion-trap system together with C.K., V.L., F.M., Y.N.V.G., P.P., and M.V. The central laser system was built by S.L., who maintained it together with P.P. Modifications were implemented by S.S. with contributions by S.L. and F.M. The simulation and calculation tools for laser cooling were developed by F.M. and S.S. F.M. performed the 3D simulations and S.S. carried out the calculations in the 1D model. T.M. reviewed the calculation approach. The PI-ICR simulations were performed by E.L. and E.M.L. utilizing a code which they developed together with A.A.K. S.S., F.M., and S.M.-E. regularly discussed the progress and directions of the project and reviewed the results together with L.S. and the entire collaboration. S.M.-E., L.S., S.R., G.N., and A.A.K. secured funding and/or resources to pursue the present project. S.S. led the writing of the paper, which was done together with S.M.-E and F.M. with contributions by E.L. All authors carefully reviewed the paper.

-
- [1] M. J. G. Borge and B. Jonson, ISOLDE past, present and future, *J. Phys. G: Nucl. Part. Phys.* **44**, 044011 (2017).
- [2] G. C. Ball, G. Hackman, and R. Krücken, The TRIUMF-ISAC facility: Two decades of discovery with rare isotope beams, *Phys. Scr.* **91**, 093002 (2016).
- [3] J. Äystö, T. Eronen, A. Jokinen, A. Kankainen, I. D. Moore, and H. Penttilä, *Three Decades of Research Using IGISOL Technique at the University of Jyväskylä* (Springer, Dordrecht, Netherlands, 2013).
- [4] J. Gerl, M. Górska, and H. J. Wollersheim, Towards detailed knowledge of atomic nuclei—the past, present and future of nuclear structure investigations at GSI, *Phys. Scr.* **91**, 103001 (2016).
- [5] G. Gaubert, C. Barué, C. Canet, J. C. Cornell, M. Dubois, M. Dupuis, C. Eleon, J. L. Flambard, R. Frigot, P. Jardin, C. Leboucher, N. Lecesne, P. Leherissier, F. Lemagnen, R. Leroy, and J. Y. Pacquet, Status report of stable and radioactive ion beam production at GANIL, *Rev. Sci. Instrum.* **79**, 02A309 (2008).
- [6] A. Gade and B. M. Sherrill, NSCL and FRIB at Michigan State University: Nuclear science at the limits of stability, *Phys. Scr.* **91**, 053003 (2016).
- [7] H. Okuno, T. Dantsuka, M. Fujimaki, N. Fukunishi, H. Hasebe, Y. Higurashi, E. Ikezawa, N. Ikoma, H. Imao, O. Kamigaito, M. Kidera, M. Komiyama, K. Kumagai, T. Maie, M. Nagase, T. Nagatomo, T. Nakagawa, M. Nakamura, J. Ohnishi, K. Ozeki *et al.*, Present status of and recent developments at RIKEN RI beam factory, *J. Phys.: Conf. Ser.* **1401**, 012005 (2020).
- [8] G. Savard, A. Levand, R. Pardo, R. Vondrasek, and B. Zabransky, The CARIBU Facility, in *Proceedings of the Conference on Advances in Radioactive Isotope Science (ARIS2014)* (The Physical Society of Japan, Tokyo, Japan, 2015).
- [9] Y. Blumenfeld, T. Nilsson, and P. V. Duppen, Facilities and methods for radioactive ion beam production, *Phys. Scr.* **2013**, 014023 (2013).
- [10] R. F. Garcia Ruiz, R. Berger, J. Billowes, C. L. Binnersley, M. L. Bissell, A. A. Breier, A. J. Brinson, K. Chrysalidis, T. E. Cocolios, B. S. Cooper, K. T. Flanagan, T. F. Giesen, R. P. de Groote, S. Franchoo, F. P. Gustafsson, T. A. Isaev, Á. Koszorus, G. Neyens, H. A. Perrett, C. M. Ricketts *et al.*, Spectroscopy of short-lived radioactive molecules, *Nature (London)* **581**, 396 (2020).
- [11] L. P. Gaffney, P. A. Butler, M. Scheck, A. B. Hayes, F. Wenander, M. Albers, B. Bastin, C. Bauer, A. Blazhev, S. Bönig, N. Bree, J. Cederkäll, T. Chupp, D. Cline, T. E. Cocolios, T. Davinson, H. De Witte, J. Diriken, T. Grahn, A. Herzan *et al.*, Studies of pear-shaped nuclei using accelerated radioactive beams, *Nature (London)* **497**, 199 (2013).

- [12] D. G. Jenkins, Recent advances in nuclear physics through on-line isotope separation, *Nat. Phys.* **10**, 909 (2014).
- [13] R. M. Dos Santos Augusto, L. Buehler, Z. Lawson, S. Marzari, M. Stachura, T. Stora, and CERN-MEDICIS collaboration, CERN-MEDICIS (Medical Isotopes Collected from ISOLDE): A new facility, *Appl. Sci.* **4**, 265 (2014).
- [14] C. Müller, K. Zhernosekov, U. Köster, K. Johnston, H. Dorrer, A. Hohn, N. T. van der Walt, A. Türler, and R. Schibli, A unique matched quadruplet of terbium radioisotopes for PET and SPECT and for alpha- and beta-radionuclide therapy: An in vivo proof-of-concept study with a new receptor-targeted folate derivative, *J. Nucl. Med.* **53**, 1951 (2012).
- [15] A. K. H. Robertson, C. F. Ramogida, P. Schaffer, and V. Radchenko, Development of ^{225}Ac radiopharmaceuticals: TRIUMF perspectives and experiences, *Curr. Radiopharm.* **11**, 156 (2018).
- [16] C. Duchemin, J. P. Ramos, T. Stora, E. Ahmed, E. Aubert, N. Audouin, E. Barbero, V. Barozier, A.-P. Bernardes, P. Bertreix, A. Boscher, F. Bruchertseifer, R. Catherall, E. Chevally, P. Christodoulou, K. Chrysalidis, T. E. Cocolios, J. Comte, B. Crepieux, M. Deschamps *et al.*, CERN-MEDICIS: A review since commissioning in 2017, *Front. Med.* **8**, 693682 (2021).
- [17] F. Herfurth, J. Dilling, A. Kellerbauer, G. Bollen, S. Henry, H.-J. Kluge, E. Lamour, D. Lunney, R. Moore, C. Scheidenberger, S. Schwarz, G. Sikler, and J. Szerypo, A linear radiofrequency ion trap for accumulation, bunching, and emittance improvement of radioactive ion beams, *Nucl. Instrum. Methods Phys. Res. Sect. A* **469**, 254 (2001).
- [18] P. Campbell, A. Nieminen, J. Billowes, P. Dendooven, K. T. Flanagan, D. H. Forest, Y. Gangrsky, J. A. R. Griffith, J. Huikari, A. Jokinen, I. D. Moore, R. Moore, H. L. Thayer, G. Tungate, S. G. Zemlyanoi, and J. Äystö, First results from laser spectroscopy on bunched radioactive beams from the JYFL ion-beam cooler, *Eur. Phys. J. A* **15**, 45 (2002).
- [19] E. Mané, J. Billowes, K. Blaum, P. Campbell, B. Cheal, P. Delahaye, K. T. Flanagan, D. H. Forest, H. Franberg, C. Geppert, T. Giles, A. Jokinen, M. Kowalska, R. Neugart, G. Neyens, W. Nörtershäuser, I. Podadera, G. Tungate, P. Vingerhoets, and D. T. Yordanov, An ion cooler-buncher for high-sensitivity collinear laser spectroscopy at ISOLDE, *Eur. Phys. J. A* **42**, 503 (2009).
- [20] T. Brunner, M. Smith, M. Brodeur, S. Ettenauer, A. Gallant, V. Simon, A. Chaudhuri, A. Lapierre, E. Mané, R. Ringle, M. Simon, J. Vaz, P. Delheij, M. Good, M. Pearson, and J. Dilling, TITAN's digital RFQ ion beam cooler and buncher, operation and performance, *Nucl. Instrum. Methods Phys. Res. Sect. A* **676**, 32 (2012).
- [21] S. Schwarz, G. Bollen, R. Ringle, J. Savory, and P. Schury, The LEBIT ion cooler and buncher, *Nucl. Instrum. Methods Phys. Res. Sect. A* **816**, 131 (2016).
- [22] B. Barquest, G. Bollen, P. Mantica, K. Minamisono, R. Ringle, S. Schwarz, and C. Sumithrarachchi, RFQ beam cooler and buncher for collinear laser spectroscopy of rare isotopes, *Nucl. Instrum. Methods Phys. Res. Sect. A* **866**, 18 (2017).
- [23] B. Barquest, J. Bale, J. Dilling, G. Gwinner, R. Kanungo, R. Krücken, and M. Pearson, Development of a new RFQ beam cooler and buncher for the CANREB project at TRIUMF, *Nucl. Instrum. Methods Phys. Res. Sect. B* **376**, 207 (2016), Proceedings of the XVIIth International Conference on Electromagnetic Isotope Separators and Related Topics (EMIS2015), Grand Rapids, MI, USA, 11-15 May 2015.
- [24] E. Haettner, W. R. Plaß, U. Czok, T. Dickel, H. Geissel, W. Kinsel, M. Petrick, T. Schäfer, and C. Scheidenberger, A versatile triple radiofrequency quadrupole system for cooling, mass separation and bunching of exotic nuclei, *Nucl. Instrum. Methods Phys. Res. Sect. A* **880**, 138 (2018).
- [25] A. Valverde, M. Brodeur, J. Clark, D. Lascar, and G. Savard, A cooler-buncher for the $N = 126$ factory at Argonne National Laboratory, *Nucl. Instrum. Methods Phys. Res. Sect. B* **463**, 330 (2020).
- [26] D. Lunney, F. Buchinger, and R. Moore, The temperature of buffer-gas cooled ions in a Paul trap, *J. Mod. Opt.* **39**, 349 (1992).
- [27] A. Kellerbauer, T. Kim, R. Moore, and P. Varfalvy, Buffer gas cooling of ion beams, *Nucl. Instrum. Methods Phys. Res. Sect. A* **469**, 276 (2001).
- [28] P. Delahaye, Analytical model of an ion cloud cooled by collisions in a Paul trap, *Eur. Phys. J. A* **55**, 83 (2019).
- [29] J. Van Schelt, D. Lascar, G. Savard, J. A. Clark, P. F. Bertone, S. Caldwell, A. Chaudhuri, A. F. Levand, G. Li, G. E. Morgan, R. Orford, R. E. Segel, K. S. Sharma, and M. G. Sternberg, First Results from the CARIBU Facility: Mass Measurements on the r -Process Path, *Phys. Rev. Lett.* **111**, 061102 (2013).
- [30] T. W. Hänsch and A. Schawlow, Cooling of gases by laser radiation, *Opt. Commun.* **13**, 68 (1975).
- [31] D. Wineland and H. Dehmelt, Proposed laser fluorescence spectroscopy on Tl^+ mono-ion oscillator, *Bull. Am. Phys. Soc.* **20** (1975).
- [32] D. J. Wineland and W. M. Itano, Laser cooling of atoms, *Phys. Rev. A* **20**, 1521 (1979).
- [33] D. J. Wineland, Nobel Lecture: Superposition, entanglement, and raising Schrödinger's cat, *Rev. Mod. Phys.* **85**, 1103 (2013).
- [34] W. D. Phillips, Nobel lecture: Laser cooling and trapping of neutral atoms, *Rev. Mod. Phys.* **70**, 721 (1998).
- [35] W. Ketterle, Nobel lecture: When atoms behave as waves: Bose-Einstein condensation and the atom laser, *Rev. Mod. Phys.* **74**, 1131 (2002).
- [36] J. Eschner, G. Morigi, F. Schmidt-Kaler, and R. Blatt, Laser cooling of trapped ions, *J. Opt. Soc. Am. B* **20**, 1003 (2003).
- [37] A. D. Ludlow, M. M. Boyd, J. Ye, E. Peik, and P. O. Schmidt, Optical atomic clocks, *Rev. Mod. Phys.* **87**, 637 (2015).
- [38] C. D. Bruzewicz, J. Chiaverini, R. McConnell, and J. M. Sage, Trapped-ion quantum computing: Progress and challenges, *Appl. Phys. Rev.* **6**, 021314 (2019).
- [39] M. S. Safronova, D. Budker, D. DeMille, D. F. Jackson Kimball, A. Derevianko, and C. W. Clark, Search for new physics with atoms and molecules, *Rev. Mod. Phys.* **90**, 025008 (2018).
- [40] C. J. Baker, W. Bertsche, A. Capra, C. Carruth, C. L. Cesar, M. Charlton, A. Christensen, R. Collister, A. C. Mathad, S. Eriksson, A. Evans, N. Evetts, J. Fajans, T. Friesen, M. C. Fujiwara, D. R. Gill, P. Grandemange, P. Granum, J. S. Hangst, W. N. Hardy *et al.*, Laser cooling of antihydrogen atoms, *Nature (London)* **592**, 35 (2021).
- [41] M. Bohman, V. Grunhofer, C. Smorra, M. Wiesinger, C. Will, M. J. Borchert, J. A. Devlin, S. Erlewein, M. Fleck, S. Gavranovic, J. Harrington, B. Latacz, A. Mooser, D. Popper,

- E. Wursten, K. Blaum, Y. Matsuda, C. Ospelkaus, W. Quint, J. Walz *et al.*, Sympathetic cooling of a trapped proton mediated by an LC circuit, *Nature (London)* **596**, 514 (2021).
- [42] C. J. Foot, *Atomic Physics*, Oxford Master Series in Atomic, Optical, and Laser Physics (Oxford University Press, Oxford, 2007).
- [43] A. Kramida, Y. Ralchenko, and J. Reader, NIST ASD Team, National Institute of Standards and Technology, NIST Atomic Spectra Database, version 5.8 (2020), <https://physics.nist.gov/asd> (accessed May 31, 2021).
- [44] R. B. Moore, A. M. G. Dezfali, P. Varfalvy, and H. Zhao, The ISOLDE Collaboration, Production, transfer and injection of charged particles in traps and storage rings, *Phys. Scr.* **1995**, 93 (1995).
- [45] K. Blaum, J. Dilling, and W. Nörtershäuser, Precision atomic physics techniques for nuclear physics with radioactive beams, *Phys. Scr.* **2013**, 014017 (2013).
- [46] P. Campbell, I. Moore, and M. Pearson, Laser spectroscopy for nuclear structure physics, *Prog. Part. Nucl. Phys.* **86**, 127 (2016).
- [47] R. Neugart, J. Billowes, M. L. Bissell, K. Blaum, B. Cheal, K. T. Flanagan, G. Neyens, W. Nörtershäuser, and D. T. Yordanov, Collinear laser spectroscopy at ISOLDE: New methods and highlights, *J. Phys. G: Nucl. Part. Phys.* **44**, 064002 (2017).
- [48] R. Wolf, D. Beck, K. Blaum, C. Böhm, C. Borgmann, M. Breitenfeldt, F. Herfurth, A. Herlert, M. Kowalska, S. Kreim, D. Lunney, S. Naimi, D. Neidherr, M. Rosenbusch, L. Schweikhard, J. Stanja, F. Wienholtz, and K. Zuber, On-line separation of short-lived nuclei by a multi-reflection time-of-flight device, *Nucl. Instrum. Methods Phys. Res. Sect. A* **686**, 82 (2012).
- [49] W. R. Plaß, T. Dickel, and C. Scheidenberger, Multiple-reflection time-of-flight mass spectrometry, *Int. J. Mass Spectrom.* **349-350**, 134 (2013), 100 years of Mass Spectrometry.
- [50] T. Dickel, W. Plaß, A. Becker, U. Czok, H. Geissel, E. Haettner, C. Jesch, W. Kinsel, M. Petrick, C. Scheidenberger, A. Simon, and M. Yavor, A high-performance multiple-reflection time-of-flight mass spectrometer and isobar separator for the research with exotic nuclei, *Nucl. Instrum. Methods Phys. Res. Sect. A* **777**, 172 (2015).
- [51] S. Eliseev, K. Blaum, M. Block, C. Droese, M. Goncharov, E. Minaya Ramirez, D. A. Nesterenko, Y. N. Novikov, and L. Schweikhard, Phase-Imaging Ion-Cyclotron-Resonance Measurements for Short-Lived Nuclides, *Phys. Rev. Lett.* **110**, 082501 (2013).
- [52] S. Eliseev, K. Blaum, M. Block, A. Dörr, C. Droese, T. Eronen, M. Goncharov, M. Höcker, J. Ketter, E. M. Ramirez, D. A. Nesterenko, Y. N. Novikov, and L. Schweikhard, A phase-imaging technique for cyclotron-frequency measurements, *Appl. Phys. B* **114**, 107 (2014).
- [53] L.-B. Wang, P. Mueller, K. Bailey, G. W. F. Drake, J. P. Greene, D. Henderson, R. J. Holt, R. V. F. Janssens, C. L. Jiang, Z.-T. Lu, T. P. O'Connor, R. C. Pardo, K. E. Rehm, J. P. Schiffer, and X. D. Tang, Laser Spectroscopic Determination of the ${}^6\text{He}$ Nuclear Charge Radius, *Phys. Rev. Lett.* **93**, 142501 (2004).
- [54] P. Mueller, I. A. Sulai, A. C. C. Villari, J. A. Alcántara-Núñez, R. Alves-Condé, K. Bailey, G. W. F. Drake, M. Dubois, C. Eléon, G. Gaubert, R. J. Holt, R. V. F. Janssens, N. Lecesne, Z.-T. Lu, T. P. O'Connor, M.-G. Saint-Laurent, J.-C. Thomas, and L.-B. Wang, Nuclear Charge Radius of ${}^8\text{He}$, *Phys. Rev. Lett.* **99**, 252501 (2007).
- [55] D. Melconian, J. Behr, D. Ashery, O. Aviv, P. Bricault, M. Dombisky, S. Fostner, A. Gorelov, S. Gu, V. Hanemaayer, K. Jackson, M. Pearson, and I. Vollrath, Measurement of the neutrino asymmetry in the β -decay of laser-cooled, polarized ${}^{37}\text{K}$, *Phys. Lett. B* **649**, 370 (2007).
- [56] K. Okada, M. Wada, T. Nakamura, A. Takamine, V. Lioubimov, P. Schury, Y. Ishida, T. Sonoda, M. Ogawa, Y. Yamazaki, Y. Kanai, T. M. Kojima, A. Yoshida, T. Kubo, I. Katayama, S. Ohtani, H. Wollnik, and H. A. Schuessler, Precision Measurement of the Hyperfine Structure of Laser-Cooled Radioactive ${}^7\text{Be}^+$ Ions Produced by Projectile Fragmentation, *Phys. Rev. Lett.* **101**, 212502 (2008).
- [57] J. A. Behr and G. Gwinner, Standard model tests with trapped radioactive atoms, *J. Phys. G: Nucl. Part. Phys.* **36**, 033101 (2009).
- [58] W. Jiang, W. Williams, K. Bailey, A. M. Davis, S.-M. Hu, Z.-T. Lu, T. P. O'Connor, R. Purtschert, N. C. Sturchio, Y. R. Sun, and P. Mueller, ${}^{39}\text{Ar}$ Detection at the 10^{-16} Isotopic Abundance Level with Atom Trap Trace Analysis, *Phys. Rev. Lett.* **106**, 103001 (2011).
- [59] C. Schneider, S. J. Schowalter, K. Chen, S. T. Sullivan, and E. R. Hudson, Laser-Cooling-Assisted Mass Spectrometry, *Phys. Rev. Appl.* **2**, 034013 (2014).
- [60] C. Schneider, S. J. Schowalter, P. Yu, and E. R. Hudson, Electronics of an ion trap with integrated time-of-flight mass spectrometer, *Int. J. Mass Spectrom.* **394**, 1 (2016).
- [61] P. C. Schmid, J. Greenberg, M. I. Miller, K. Loeffler, and H. J. Lewandowski, An ion trap time-of-flight mass spectrometer with high mass resolution for cold trapped ion experiments, *Rev. Sci. Instrum.* **88**, 123107 (2017).
- [62] N. Deb, L. L. Pollum, A. D. Smith, M. Keller, C. J. Rennick, B. R. Heazlewood, and T. P. Softley, Coulomb crystal mass spectrometry in a digital ion trap, *Phys. Rev. A* **91**, 033408 (2015).
- [63] T. Manovitz, R. Shaniv, Y. Shapira, R. Ozeri, and N. Akerman, Precision Measurement of Atomic Isotope Shifts using a Two-Isotope Entangled State, *Phys. Rev. Lett.* **123**, 203001 (2019).
- [64] P.-G. Reinhard, W. Nazarewicz, and R. F. Garcia Ruiz, Beyond the charge radius: The information content of the fourth radial moment, *Phys. Rev. C* **101**, 021301(R) (2020).
- [65] S. Sels, P. Fischer, H. Heylen, V. Lagaki, S. Lechner, F. Maier, P. Plattner, M. Rosenbusch, F. Wienholtz, R. Wolf, W. Nörtershäuser, L. Schweikhard, and S. Malbrunot-Ettenauer, First steps in the development of the multi ion reflection apparatus for collinear laser spectroscopy, *Nucl. Instrum. Methods Phys. Res. Sect. B* **463**, 310 (2020).
- [66] F. M. Maier, P. Fischer, H. Heylen, V. Lagaki, S. Lechner, P. Plattner, S. Sels, F. Wienholtz, W. Nörtershäuser, L. Schweikhard, and S. Malbrunot-Ettenauer, Simulations of a proof-of-principle experiment for collinear laser spectroscopy within a multi-reflection time-of-flight device, *Hyperfine Interact.* **240**, 54 (2019).
- [67] V. Lagaki, P. Fischer, H. Heylen, F. Hummer, S. Lechner, M. F.M., P. Plattner, M. Rosenbusch, F. Wienholtz, R. Wolf, W. Nörtershäuser, L. Schweikhard, and S. Malbrunot-Ettenauer,

- Stray-light suppression for the MIRACLS proof-of-principle experiment, *Acta Phys. Pol. B* **51**, 571 (2020).
- [68] V. Lagaki, H. Heylen, I. Belosevic, P. Fischer, C. Kanitz, S. Lechner, F. Maier, W. Nörtershäuser, P. Plattner, M. Rosenbusch, S. Sels, L. Schweikhard, M. Vilen, F. Wienholtz, R. Wolf, and S. Malbrunot-Ettenauer, An accuracy benchmark of the MIRACLS apparatus: Conventional, single-passage collinear laser spectroscopy inside a MR-ToF device, *Nucl. Instrum. Methods Phys. Res. Sect. A* **1014**, 165663 (2021).
- [69] S. Lechner, P. Fischer, H. Heylen, V. Lagaki, F. Maier, P. Plattner, M. Rosenbusch, S. Sels, F. Wienholtz, R. N. Wolf, W. Nörtershäuser, L. Schweikhard, and S. Malbrunot-Ettenauer, Fluorescence detection as a new diagnostics tool for electrostatic ion beam traps, *Hyperfine Interact.* **240**, 95 (2019).
- [70] L. M. Bartels, Increasing electron emission rates in an offline electron impact Mg⁺ ion source for laser spectroscopy of radioactive ions, bachelor's thesis, Georg-August-Universität Göttingen, Germany 2018.
- [71] T. Murböck, S. Schmidt, Z. Anelkovic, G. Birkel, W. Nörtershäuser, and M. Vogel, A compact source for bunches of singly charged atomic ions, *Rev. Sci. Instrum.* **87**, 043302 (2016).
- [72] D. Leimbach, Radioactive negative ions: Production and laser spectroscopy at ISOLDE, Ph.D. thesis, Johannes Gutenberg Universitaet Mainz, 2021.
- [73] U. Köster, ISOLDE target and ion source chemistry, *Radiochimica Acta* **89**, 749 (2001).
- [74] E. Kugler, The ISOLDE facility, *Hyperfine Interact.* **129**, 23 (2000).
- [75] R. Kersevan and J.-L. Pons, Introduction to MOLFLOW+: New graphical processing unit-based Monte Carlo code for simulating molecular flows and for calculating angular coefficients in the compute unified device architecture environment, *J. Vac. Sci. Technol. A* **27**, 1017 (2009).
- [76] F. Wienholtz, K. Blaum, J. Karthein, D. Lunney, S. Malbrunot-Ettenauer, V. Manea, M. Mougeot, L. Schweikhard, T. Steinsberger, and R. Wolf, Improved stability of multi-reflection time-of-flight mass spectrometers through passive and active voltage stabilization, *Nucl. Instrum. Methods Phys. Res. Sect. B* **463**, 348 (2020).
- [77] P. Fischer and L. Schweikhard, Multiple active voltage stabilizations for multi-reflection time-of-flight mass spectrometry, *Rev. Sci. Instrum.* **92**, 063203 (2021).
- [78] R. Wolf, F. Wienholtz, D. Atanasov, D. Beck, K. Blaum, C. Borgmann, F. Herfurth, M. Kowalska, S. Kreim, Y. A. Litvinov, D. Lunney, V. Manea, D. Neidherr, M. Rosenbusch, L. Schweikhard, J. Stanja, and K. Zuber, ISOLTRAP's multi-reflection time-of-flight mass separator/spectrometer, *Int. J. Mass Spectrom.* **349-350**, 123 (2013).
- [79] M. Nötzold, S. Z. Hassan, J. Tauch, E. Endres, R. Wester, and M. Weidemüller, Thermometry in a multipole ion trap, *Appl. Sci.* **10**, 5264(2020).
- [80] J. B. Wübbena, S. Amairi, O. Mandel, and P. O. Schmidt, Sympathetic cooling of mixed-species two-ion crystals for precision spectroscopy, *Phys. Rev. A* **85**, 043412 (2012).
- [81] M. Guggemos, D. Heinrich, O. A. Herrera-Sancho, R. Blatt, and C. F. Roos, Sympathetic cooling and detection of a hot trapped ion by a cold one, *New J. Phys.* **17**, 103001 (2015).
- [82] D. Manura and D. Dahl, SIMION 8.1 User Manual (2008).
- [83] D. Manura, SIMION HS1 collision model REV4 (2007).
- [84] J. H. Wesenberg, R. J. Epstein, D. Leibfried, R. B. Blakestad, J. Britton, J. P. Home, W. M. Itano, J. D. Jost, E. Knill, C. Langer, R. Ozeri, S. Seidelin, and D. J. Wineland, Fluorescence during Doppler cooling of a single trapped atom, *Phys. Rev. A* **76**, 053416 (2007).
- [85] T. Murböck, S. Schmidt, G. Birkel, W. Nörtershäuser, R. C. Thompson, and M. Vogel, Rapid crystallization of externally produced ions in a Penning trap, *Phys. Rev. A* **94**, 043410 (2016).
- [86] S. George, K. Blaum, M. Block, M. Breitenfeldt, M. Dworschak, F. Herfurth, A. Herlert, M. Kowalska, M. Kretzschmar, E. M. Ramirez, D. Neidherr, S. Schwarz, and L. Schweikhard, Damping effects in Penning trap mass spectrometry, *Int. J. Mass Spectrom.* **299**, 102 (2011).
- [87] L. M. Chanin and M. A. Biondi, Mobilities of mercury ions in helium, neon, and argon, *Phys. Rev.* **107**, 1219 (1957).
- [88] W. Ertmer, R. Blatt, J. L. Hall, and M. Zhu, Laser Manipulation of Atomic Beam Velocities: Demonstration of Stopped Atoms and Velocity Reversal, *Phys. Rev. Lett.* **54**, 996 (1985).
- [89] M. Reiter, S. A. S. Andrés, J. Bergmann, T. Dickel, J. Dilling, A. Jacobs, A. Kwiatkowski, W. Plaß, C. Scheidenberger, D. Short, C. Will, C. Babcock, E. Dunling, A. Finlay, C. Hornung, C. Jesch, R. Klawitter, B. Kootte, D. Lascar, E. Leistenschneider *et al.*, Commissioning and performance of TITAN's multiple-reflection time-of-flight mass-spectrometer and isobar separator, *Nucl. Instrum. Methods Phys. Res. Sect. A* **1018**, 165823 (2021).
- [90] T. Dickel, M. I. Yavor, J. Lang, W. R. Plaß, W. Lippert, H. Geissel, and C. Scheidenberger, Dynamical time focus shift in multiple-reflection time-of-flight mass spectrometers, *Int. J. Mass Spectrom.* **412**, 1 (2017).
- [91] R. N. Wolf, G. Marx, M. Rosenbusch, and L. Schweikhard, Static-mirror ion capture and time focusing for electrostatic ion-beam traps and multi-reflection time-of-flight mass analyzers by use of an in-trap potential lift, *Int. J. Mass Spectrom.* **313**, 8 (2012).
- [92] J. Dilling, K. Blaum, M. Brodeur, and S. Eliseev, Penning-trap mass measurements in atomic and nuclear physics, *Annu. Rev. Nucl. Part. Sci.* **68**, 45 (2018).
- [93] M. Brodeur, V. Ryjkov, T. Brunner, S. Ettenauer, A. Gallant, V. Simon, M. Smith, A. Lapiere, R. Ringle, P. Delheij, M. Good, D. Lunney, and J. Dilling, Verifying the accuracy of the TITAN Penning-trap mass spectrometer, *Int. J. Mass Spectrom.* **310**, 20 (2012).
- [94] E. M. Lykiardopoulou, C. Izzo, E. Leistenschneider, A. A. Kwiatkowski, and J. Dilling, Towards high precision mass measurements of highly charged ions using the phase-imaging ion-cyclotron-resonance technique at TITAN, *Hyperfine Interact.* **241**, 37 (2020).
- [95] D. A. Nesterenko, T. Eronen, A. Kankainen, L. Canete, A. Jokinen, I. D. Moore, H. Penttilä, S. Rinta-Antila, A. de Roubin, and M. Vilen, Phase-imaging ion-cyclotron-resonance technique at the JYFLTRAP double Penning trap mass spectrometer, *Eur. Phys. J. A* **54**, 154 (2018).
- [96] V. Batteiger, S. Knünz, M. Herrmann, G. Saathoff, H. A. Schüssler, B. Bernhardt, T. Wilken, R. Holzwarth, T. W. Hänsch, and T. Udem, Precision spectroscopy of the 3s–3p fine-structure doublet in Mg⁺, *Phys. Rev. A* **80**, 022503 (2009).

- [97] K. König, P. Imgram, J. Krämer, B. Maaß, K. Mohr, T. Ratajczyk, F. Sommer, and W. Nörtershäuser, On the performance of wavelength meters: Part 2- frequency-comb based characterization for more accurate absolute wavelength determinations, *Appl. Phys. B* **126**, 86 (2020).
- [98] M. Verlinde, K. Dockx, S. Geldhof, K. König, D. Studer, T. E. Cocolios, R. P. de Groote, R. Ferrer, Y. Kudryavtsev, T. Kieck, I. Moore, W. Nörtershäuser, S. Raeder, P. Van den Bergh, P. Van Duppen, and K. Wendt, On the performance of wavelength meters: Part 1-consequences for medium-to-high-resolution laser spectroscopy, *Appl. Phys. B* **126**, 85 (2020).
- [99] W. Nörtershäuser, D. Tiedemann, M. Žáková, Z. Andjelkovic, K. Blaum, M. L. Bissell, R. Cazan, G. W. F. Drake, C. Geppert, M. Kowalska, J. Krämer, A. Krieger, R. Neugart, R. Sánchez, F. Schmidt-Kaler, Z.-C. Yan, D. T. Yordanov, and C. Zimmermann, Nuclear Charge Radii of $^{7,9,10}\text{Be}$ and the One-Neutron Halo Nucleus ^{11}Be , *Phys. Rev. Lett.* **102**, 062503 (2009).
- [100] T. Otsuka, A. Gade, O. Sorlin, T. Suzuki, and Y. Utsuno, Evolution of shell structure in exotic nuclei, *Rev. Mod. Phys.* **92**, 015002 (2020).
- [101] B. H. Wildenthal and W. Chung, Collapse of the conventional shell-model ordering in the very-neutron-rich isotopes of Na and Mg, *Phys. Rev. C* **22**, 2260 (1980).
- [102] M. Hammen, W. Nörtershäuser, D. L. Balabanski, M. L. Bissell, K. Blaum, I. Budinčević, B. Cheal, K. T. Flanagan, N. Frömmgen, G. Georgiev, C. Geppert, M. Kowalska, K. Kreim, A. Krieger, W. Nazarewicz, R. Neugart, G. Neyens, J. Papuga, P. G. Reinhard, M. M. Rajabali, S. Schmidt, and D. T. Yordanov, From Calcium to Cadmium: Testing the Pairing Functional Through Charge Radii Measurements of $^{100-130}\text{Cd}$, *Phys. Rev. Lett.* **121**, 102501 (2018).
- [103] D. T. Yordanov, D. L. Balabanski, M. L. Bissell, K. Blaum, I. Budinčević, B. Cheal, K. Flanagan, N. Frömmgen, G. Georgiev, C. Geppert, M. Hammen, M. Kowalska, K. Kreim, A. Krieger, J. Meng, R. Neugart, G. Neyens, W. Nörtershäuser, M. M. Rajabali, J. Papuga, S. Schmidt, and P. W. Zhao, Simple Nuclear Structure in $^{111-129}\text{Cd}$ from Atomic Isomer Shifts, *Phys. Rev. Lett.* **116**, 032501 (2016).
- [104] T. Otsuka, T. Suzuki, M. Honma, Y. Utsuno, N. Tsunoda, K. Tsukiyama, and M. Hjorth-Jensen, Novel Features of Nuclear Forces and Shell Evolution in Exotic Nuclei, *Phys. Rev. Lett.* **104**, 012501 (2010).
- [105] I. Counts, J. Hur, D. P. L. Aude Craik, H. Jeon, C. Leung, J. C. Berengut, A. Geddes, A. Kawasaki, W. Jhe, and V. Vuletić, Evidence for Nonlinear Isotope Shift in Yb^+ Search for New Boson, *Phys. Rev. Lett.* **125**, 123002 (2020).
- [106] Isolde Target Team, ISOLDE Yield database (2020).
- [107] R. P. de Groote, J. Billowes, C. L. Binnorsley, M. L. Bissell, T. E. Cocolios, T. Day Goodacre, G. J. Farooq-Smith, D. V. Fedorov, K. T. Flanagan, S. Franchoo, R. F. Garcia Ruiz, W. Gins, J. D. Holt, Á. Koszorús, K. M. Lynch, T. Miyagi, W. Nazarewicz, G. Neyens, P.-G. Reinhard, S. Rothe *et al.*, Measurement and microscopic description of odd-even staggering of charge radii of exotic copper isotopes, *Nat. Phys.* **16**, 620 (2020).
- [108] R. Neugart, Lasers in nuclear physics—a review, in *Exotic Nuclei and Atomic Masses*, edited by J. Äystö, P. Dendooven, A. Jokinen, and M. Leino (Springer, Berlin, 2003), pp. 69–73.
- [109] S. Kaufman, High-resolution laser spectroscopy in fast beams, *Opt. Commun.* **17**, 309 (1976).
- [110] H. Heylen, C. S. Devlin, W. Gins, M. L. Bissell, K. Blaum, B. Cheal, L. Filippin, R. F. Garcia Ruiz, M. Godefroid, C. Gorges, J. D. Holt, A. Kanellakopoulos, S. Kaufmann, A. Koszorús, K. König, S. Malbrunot-Ettenauer, T. Miyagi, R. Neugart, G. Neyens, W. Nörtershäuser *et al.*, High-resolution laser spectroscopy of $^{27-32}\text{Al}$, *Phys. Rev. C* **103**, 014318 (2021).
- [111] P. Micke, T. Leopold, S. A. King, E. Benkler, L. J. Spieß, L. Schmöger, M. Schwarz, J. R. Crespo López-Urrutia, and P. O. Schmidt, Coherent laser spectroscopy of highly charged ions using quantum logic, *Nature (London)* **578**, 60 (2020).
- [112] Y. Meng and L. Du, Study on the high-efficiency sympathetic cooling of mixed ion system with a large mass-to-charge ratio difference in a dual radio-frequency field by numerical simulations, *Eur. Phys. J. D* **75**, 19 (2021).
- [113] C. J. Campbell, A. V. Steele, L. R. Churchill, M. V. DePalatis, D. E. Naylor, D. N. Matsukevich, A. Kuzmich, and M. S. Chapman, Multiply Charged Thorium Crystals for Nuclear Laser Spectroscopy, *Phys. Rev. Lett.* **102**, 233004 (2009).